Theoretical Studies on Water Splitting Using Transition Metal Complexes

Ying Wang

王英

Doctoral Thesis in Theoretical Chemistry & Biology

School of Biotechnology

Royal Institute of Technology

Stockholm, Sweden 2014

Theoretical Studies on Water Splitting Using Transition Metal Complexes
Thesis for Doctoral Degree
Division of Theoretical Chemistry & Biology
School of Biotechnology
Royal Institute of Technology (KTH)
Stockholm, Sweden 2014

ISBN 978-91-7595-069-3
ISSN 1654-2312
TRITA-BIO Report 2014:6
Printed by Universitetsservice US-AB
Stockholm, Sweden, 2014

Dedicated To my family

Abstract

Encouragement Can Work Miracles

Theoretical studies on artificial water splitting processes (water oxidation and proton reduction) are presented in this thesis. A major challenge facing humanity is the development of renewable sources of energy to replace fossil fuels, and solar energy is considered to be an inexhaustible and decentralized natural resource. In fact, the fossil-fuel based energy consumed nowadays derives from solar energy harvested by photosynthetic organisms. Along with the rapid development of research on utilizing of solar energy, which is a renewable, green and clean energy source, many research groups are focusing their attention on artificial photosynthesis systems inspired by photosystem **I** and **II** to achieve efficient light-to-chemical energy transformation.

The overall reaction in these artificial systems is to store energy of sunlight in a fuel by rearranging the chemical bonds of water to form molecular oxygen and hydrogen. In general, artificial water splitting can be separated into two half reactions, catalytic water oxidation and catalytic proton reduction. There is great interest and demand to understand the detailed mechanisms of these two key parts. DFT (density functional theory) in particular, has proven to be a powerful tool in exploring reaction mechanisms. The B3LYP and M06 functionals were employed to provide theoretical explanations of these two important reactions in this thesis.

Many efficient water oxidation catalysts (WOCs) based on Ru, Co, Fe, Ir, etc., have been reported over the last several years for the water oxidation reaction. The discovery of mononuclear ruthenium WOCs carrying anionic ligands is one of the major recent breakthroughs. WOCs bearing anionic ligands are able to efficiently drive catalytic water oxidation with relatively high Turnover Numbers (TON) and Turnover Frequencies (TOF). Therefore, the influence of anionic ligands attracted our attention. We carried out a detailed investigation on this effect, and attempt to propose a full mechanism of the catalytic water. We found 1) that the anionic ligands exert a promoting influence on the ligand exchange between picoline and water, which facilitates the formation of aqua-Ru complex, 2) that the anionic ligands facilitate the complex to access higher oxidation states, which is necessary for the OO bond formation, and 3) the mechanism of OO bond formation, a key step for O_2 generation.

For the hydrogen generation/oxidation, the transport or movement of protons is vital and interesting in many biological and chemical processes, including the hydrogen uptake/production, the reduction of CO_2 to formate, and the reduction of O_2 to water. It is often related to energy storage and utilization. However, the details of these processes are still ambiguous. In most natural hydrogenase enzymes or synthetic catalysts based on iron or nickel, the incorporation of a pendant amine is a frequently occurring feature. This internal amine base facilitates this proton transfer as a proton relay. Our calculated results showed that the internal base allows for a splitting of one high enthalpy-high entropy barrier into two: one with a high enthalpy-low entropy barrier and the other with a low enthalpy-high entropy barrier, resulting in a low free energy of activation for proton transfer. One mechanistic study on modeling of the one $Fe^{II}Fe^{I}$ complex, which is the H_{ox} state (characterized by an open coordination site on the distal iron and paramagnetic), for H_2 activation was also completed in this thesis. It implies that the most favorable reaction path involves a rotation of the bridging CO to an apical position firstly, followed by H_2 activation to generate a bridging hydride intermediate with the help of the internal base. Our results can shed light on the molecular details of hydrogen generation, and serve as a guideline in the development of new catalysts, not only for proton reduction catalysts, but also for any process that involves proton transfer from a metal hydride to an external base, such as C-H activation and functionalization catalysts.

A thorough understanding of the mechanistic details of water splitting is crucial for the rational design of artificial model complexes for both water oxidation and hydrogen generation/oxidation. Minor modifications of model complexes would lead to a lower barrier for rate-determining step in the overall catalytic cycle, and can construct artificial water splitting systems with improved performance.

The work presented in the thesis was carried out at the Division of Theoretical Chemistry & Biology, School of Biotechnology, Royal Institute of Technology (KTH), Sweden.

List of papers included in the thesis

Paper I Water Oxidation Catalysis: Influence of Anionic Ligands upon the Redox Properties and Catalytic Performance of Mononuclear Ruthenium Complexes.

Lianpeng Tong, **Ying Wang**, Lele Duan, Yunhua Xu, Xiao Cheng, Andreas Fischer, Mårten S. G. Ahlquist*, and Licheng Sun*.

Inorg. Chem., **2012**, *51*, 3388–3398.

Paper II Where does the Water go? A Computational study on reactivity a Ruthenium Oxo complex (bpc)(bpy)$Ru^{V}O$.

Ying Wang and Mårten S. G. Ahlquist*.

Phys. Chem. Chem. Phys., **2014**, DOI: 10.1039/C4CP01183J.

Paper III A Computational Study of the Mechanism for Water Oxidation by (bpc)(bpy)$Ru^{II}OH_2$.

Ying Wang, and Mårten S. G. Ahlquist*.

Dalton Trans., **2014**, Submitted.

Paper IV Pendant Amine Bases Speed up Proton Transfers to Metals by Splitting the Barriers.

Ying Wang, Mei Wang, Licheng Sun, and Mårten S. G. Ahlquist*.

Chem. Commun., **2012**, *48*, 4450-4452.

Paper V Mechanistic Studies on Proton Transfer in a [FeFe] Hydrogenase Mimic Complex.

Ying Wang and Mårten S. G. Ahlquist*.

Dalton Trans., **2013**, *42*, 7816-7822.

Paper VI Catalytic Activation of H_2 under Mild Conditions by an [FeFe]-Hydrogenase Model via an Active μ-Hydride Species.

Ning Wang, Mei Wang*, **Ying Wang**, Dehua Zheng, Hongxian Han, Mårten S. G. Ahlquist, Licheng Sun*.

J. Am. Chem.Soc. **2013**, *135*, 13688-13691.

Comments on my contribution to the papers included.

As the first author, I was responsible for the calculations and the writing of the first draft for Paper **II**, Paper **III**, Paper **IV** and Paper **V**. As the co-author, I was responsible for the theoretical calculations, discussion and revision of Paper **I**, and Paper **VI**.

List of main publications not included in the thesis

Paper I Electrochemical and spectroscopic characterization of a dicobalt macrocyclic Pacman complex in the catalysis of the oxygen reduction reaction in acid media.

Qinggang He*, Xiao Cheng, **Ying Wang**, Ruimin Qiao, Wanli Yang, Jinghua Guo.

J. Porphyrins Phthalocyanines. **2013**, 17, 252-258.

Paper II The alkene epoxidation catalysts [Ru(pdc)(tpy)] and [Ru(pdc)(pybox)] revisited: revealing an unique RuIV=O structure from a dimethyl sulfoxide coordinating complex.

Ying Wang, Lele Duan, Lei Wang, Mikhail Gorlov, Licheng Sun*, and Mårten S. G. Ahlquist*.

Chem. Eur. J., **2014**, In manuscript.

Paper III A DFT Study: The Reaction Mechanism for Hydrogen Oxidation Catalyzed by an Iron Complex with Pendant Amine Ligand.

Liqin Xue, **Ying Wang**, Mårten S. G. Ahlquist*.

Chem. Sci., **2014**, In manuscript.

Paper IV Superefficient Water Oxidation Catalysts Based on Ruthenium Complexes with Halogen Substitute Ligands.

Lei Wang, Lele Duan, **Ying Wang**, Hong Chen, Mårten S. G. Ahlquist, and Licheng Sun*.

Angew. Chem. Int. Ed., **2014**, Submitted.

Paper V Improved performance on Hydrogen Activation by Minor modifications of Iron-based Model Complexes – A Computational Study.

Ying Wang and Mårten S. G. Ahlquist*.

In manuscript.

Paper VI Towards Electrochemical Nucleophilic Synthesis of 4-[18F]fluoro-catechol.

Qinggang He, **Ying Wang**, Ines Alfeazi, Saman Sadeghi*.

Applied Radiation and Isotopes, **2014***,* Accepted.

Abbreviations and acronyms

bpp	bis(2-pyridyl)-3,5-pyrazolate
bpy	bipyridine
dpp	2,9-dipyrid-2'-yl-1,10-phenanthroline
isoq	isoquinoline
pbn	2,2'-[4-(tert-butyl)pyridine-2,6-diyl]bis(1,8-naphthyridine)
pic	4-picoline
py	pyridine
tpy	2,2′:6′,2″-terpyridine
B3LYP	Becke, three-parameter, Lee-Yang-Parr
BLYP	Becke-Lee-Yang-Parr
CAES	Compressed Air Energy Storage
CCSD	Coupled Cluster Singles and Doubles
CI	Configuration Interaction
CpI	Clostridium pasteurianum I
DdH	Desulfovibrio desulfuricans Hildenborough
DFT	Density Functional Theory
GGAs	Generalized gradient approximations
OEC	Oxygen Evolving Complex
H_2bda	2,2'-bipyridine-6,6'-dicarboxylic acid
H_2hqc	8-hydroxyquinoline-2-carboxylic acid
H_2pdc	2,6-pyridine-dicarboxylic acid
HF	Hartree-Fock
I2M	Interaction between 2 M-O Units
LDA	local density approximation
MCSCF	Multi-Configuration Self-Consistent Field
MP_n	Many-body Perturbation theory
M06	Minnesota density functional
NHE	Normal Hydrogen Electrode
P680	Triad composed of a multimer of Chlorophylls
PBE	Gradient-corrected correlation functional of Perdew, Burke and Ernzerhof

PCET	Proton-Coupled Electron Transfer
TOF	TurnOver Frequency
TON	TurnOver Number
PRC	Proton Reduction Catalyst
PS-II	PhotoSystem II
TST	Transition State Theory
Tyrz	D1-tyrosine 161
WNA	Water Nucleophilic Attack
WOC	Water Oxidation Catalyst
XC	Exchange-Correlation
ZPE	Zero Point Energy

Acknowledgments

First of all, I would like to express my sincere gratitude to my supervisor Prof. Mårten Ahlquist, thanks a lot for his guidance and insightful suggestions, and the work of this thesis would not have been completed without the great help from him and I really appreciated it.

Great thanks to Prof. Hans Ågren, for giving me this precious opportunity studying in this department, and creating such a wonderful and nice environment for us. Great thanks to Prof Yi Luo, for his kind help when I firstly came to this department, and valuable advices all the time.

Many thanks to Prof. Licheng Sun, Prof. Mei Wang, Dr. Lele Duan, Dr. Lianpeng Tong, Lei Wang and Xiao Cheng for their pleasant cooperation and useful discussion.

Many thanks to Prof. Boris Minaev, Prof. Ying Fu, Prof. Faris Gel'mukhanov, Prof. Yaoquan Tu, Prof. Zilvinas Rinkevicius, Prof. Olav Vahtras and Dr. Radovan Bast for their wonderful lectures.

Many thanks to Dr. Liqin Xue, Dr. Rocío Marcos, Dr. Rocío Sánchez and Irina Osadchuk for their useful discussion and pleasant time we spent together.

Many thanks to my colleagues in this department, they are Dr. Weijie Hua, Dr. Chunze Yuan, Jing Huang, Wei Hu, Dr. Xiuneng Song, Dr. Peng Cui, Dr. Yuejie Ai, Yan Wang, Xianqiang Sun, Dr. Li Gao, Dr. Quan Miao, Dr. Xin Li (86), Dr. Guangjun Tian, Li Li, Xinrui Cao, Xin Li(82), Dr. Guangping Zhang, Ignat Harczuk, Xu Wang, Guanglin Kuang, Zhengzhong Kang, Zuyong Gong, Dr. Robert Zalesny, Jaime Axel Rosal Sandberg, Asghar Jamshidi Zavaraki, Dr. Bogdan Frecus, Junfeng Li, Dr Zhihui Chen, Dr Xiangjun Shang, Dr. Xifeng Yang, Hongbao Li, Fuming Ying, Dr. Arul Murugan, Dr. Kestutis Aidas, Dr. Johannes Niskanen and Kayathri Rajarathinam.

Thanks to Prof. Mårten Ahlquist, Dr. Liqin Xue, Dr. Rocío Marcos, Dr Chunze Yuan and Jing Huang for proof reading of this thesis.

Special thanks are sent to Dr. Xing Chen and Dr. Qiang Fu for their patient instruction on the basic knowledge of theoretical chemistry, and persistent encouragement as well, this is quite helpful and important for me to carry on.

Special thanks to Dr. Lili Lin, Yong Ma, Lu Sun, Dr. Qiong Zhang, Dr. Sai Duan, Ce Song, Yongfei Ji, Dr. Junkuo Gao, and Lijun Liang for their kind help and pleasant cooperation on courses I attended.

I would also like to thank the Erasmus Mundus TANDEM for financial support.

Last but not least, great thanks to my family, I could not make this if lack of your endless love and strong support all the time, I will love you all always and forever, and keep following my dream no matter whatever comes along.

Contents

Chapter 1

Introduction

1.1 A Brief Introduction to Global Energy Consumption.

Energy consumption demand is predicted to rise significantly, up to 28-35 TW by 2050, from the present state of about 16.3 TW.[1,2] However the natural supplies of the one of the major sources of energy, petroleum, are decreasing. In addition, the generation of CO_2 is considered to be the main factor of potentially catastrophic consequences on the environment. Hence, access to sustainable and clean energy will clearly be a major problem already in the next decades. The sun will play an irreplaceable role in sustainable energy production, and it is actually the original source of most of the energy we are using now.

The solar energy, as an abundant and sustainable form of energy, is gaining our attention and we need to find ways to store the energy efficiently. Photovoltaic cells are usually what comes to people's minds when talking about solar energy usage, however the development of them meets the limits of daylight-dependent nature, as well as the financial costs. Light-driven catalytic water splitting, which captures the energy of sunlight by storing into the chemical bonds of hydrogen, is gaining more and more attention. Compared to photovoltaic cells, where the solar energy is converted into electricity first, then converted again into the chemical energy for storage (this second conversion results in a necessary loss of energy), the solar energy can be directly converted and stored by light-driven water splitting. Furthermore, the energy obtained from light-driven splitting would be carbon-neutral and environmentally benign.

1.2 Natural Photosynthesis.

To convert the solar energy to chemical energy effectively nature provides a blueprint in the photosynthesis.[3,4] Photosynthesis, which occurs in plants and some algae, is a chemical process of converting the solar energy into chemical forms and storing it in the chemical bonds of organic molecules, and those organic molecules are the building blocks of oil, coal, gas and all living organisms. The entire process requires the energy from sunlight, carbon dioxide, and water, all of them abundant, inexpensive, and easy to fetch. The products of the natural photosynthesis are carbohydrates and oxygen, which are vital and essential to the survival and development of mankind.

Although photosynthesis takes place in many different ways in different environments, the key features of the process are similar.[5] From these features we can make a general picture about this important process (Figure 1.1).

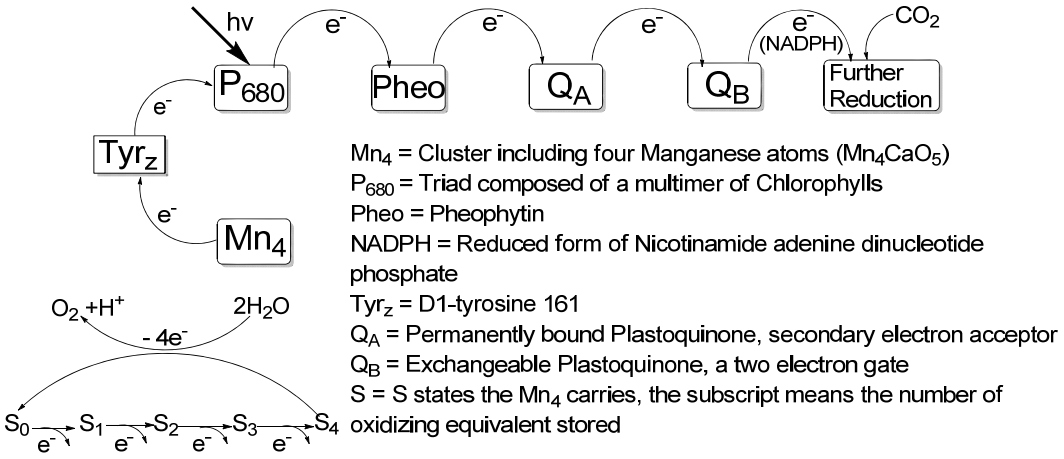

Figure 1.1 *A Brief overview of Photosynthesis in nature.*

Photosynthesis starts with the initial light-harvesting process by the photosensitizer P680, which is a triad composing of a multimer of chlorophylls. Once the energy is absorbed, P680 reaches its excited state P680* and it transfers electrons to a permanently bound plastoquinone molecule, Q_A, via a pheophytin molecule. By binding a plastoquinone molecule at the Q_B site, the transferring electrons finally go to the plastoquinone molecules in the membrane, where a two-electron reduction from plastoquinone to plastoquinol occurs. Here Q_B functions as a two-electron gate. In fact, this electron transfer is proton-coupled between redox cofactors along the photosynthetic chain, which allows further spatial charge separation. And the reduced form of nicotinamide adenine dinucleotide phosphate (NADPH) is produced by ferredoxin-$NADP^+$ reductase in

the last step of the electron transfer chain. Following this process is the multi-electronic redox catalysis, namely as the Calvin-Benson Cycle, which completes the reduction of captured CO_2 by using the newly formed NADPH, and forms three-carbon sugars, which can be combined to generate glucose and higher carbohydrates later.

On the other side, after transferring one electron to the electron acceptor part, the oxidized $P680^+$ becomes one of nature's strongest oxidizing species, with a potential of 1.2V vs. NHE. It can oxidize the tyrosine residue Tyrz in a multiphasic process, and the oxidized Tyrz will be reduced by a manganese cluster quickly, which is the oxygen-evolving $CaMn_4$ complex (OEC) [6] of photosystem II. The OEC achieves turnover numbers (TON) of 180,000 molecules of O_2 per site and turnover frequencies (TOF) of 100-400 s^{-1} [7]. The oxidized manganese cluster, which includes four manganese atoms can in turn oxidize water nearby. By four successive charge separations the manganese cluster accumulates four oxidizing equivalents, which are named S_1 to S_4, (the subscript indicates the number of oxidizing equivalents it stored), and it is able to split two water molecules into oxygen and protons. The electrons that are used for the Calvin-Benson Cycle originates from the oxidation of water.

1.3 Artificial Photosynthesis.

The development of a new approach based on the use of two sustainable resources, sunlight and water, is an attractive solution to the future energy supply of the world. The importance and success of photosynthesis has inspired scientists to construct artificial photosynthetic system for solar energy conversion.[8-9] The overall reaction in these systems is water splitting (Figure 1.2), which is breaking the O-H bonds in water and forming molecular hydrogen and oxygen assisted by corresponding catalysts.

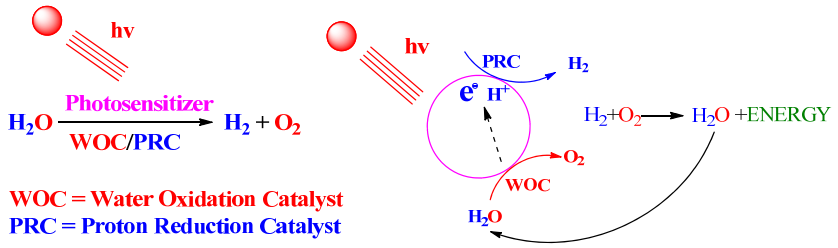

Figure 1.2 *Light-driven catalytic water splitting.*

The reaction of water splitting can be typically separated into its two half reactions: catalytic water oxidation and catalytic proton reduction. Water splitting

is an uphill energy transformation (multi-electron process coupled with a multiple proton transfers), which is expressed as Eq. 1-1. [10]

$$2H_2O \xrightarrow{h\nu} O_2 + 2H_2 \quad \Delta G^\circ = 4.92\ eV\ (113\ kcal/mol) \tag{1-1}$$

1) Catalytic water oxidation (Eq. 1-2):

$$2H_2O \xrightarrow[\text{Photo-sensitizer}]{\text{hv, WOC}} O_2 + 4e^- + 4H^+ \tag{1-2}$$

This reaction is an essential part of water splitting, since the reaction produces O_2, where water is the environmentally benign and abundant electron source that could satisfy the scale of the process required to meet the worldwide energy demands. The net half reaction is water oxidation to produce oxygen, with electrons and protons generated as "by-products". This reaction can convert the solar energy into chemical energy, which is completed with the involvement of photo-sensitizers and water oxidation catalysts. The $[Ru(bpy)_3]^{2+}$ (bpy is 2,2'-bipyridine) complex is a frequently used photo-sensitizer. After absorption of energy from sunlight, it reaches its excited state $[Ru(bpy)_3]^{2+*}$, which is a strong oxidant, and it can oxidize the corresponding water oxidation catalysts (Ru, Ir, Co complexes), which then completes the water oxidation process.

2) Catalytic proton reduction (Eq. 1-3):

$$2H^+ + 2e^- \xrightarrow[\text{Photo-sensitizer}]{\text{hv, PRC}} H_2 \tag{1-3}$$

The generated protons and electrons from catalytic water oxidation can be used to produce hydrogen. The process is assisted by proton reduction catalysts (PRC). Here $[Ru(bpy)_3]^{2+}$ can be also used as a photo-sensitizer, which is excited by sunlight to $[Ru(bpy)_3]^{2+*}$. In laboratory setups the sensitizer is then rapidly reduced to $[Ru(bpy)_3]^{1+}$ by a sacrificial electron donor such as ascorbate. After transferring the electrons to a proton reduction catalyst, such as a hydrogenase, it returns to $[Ru(bpy)_3]^{2+}$ and the electrons transferred to the catalysts are used to reduce protons to produce hydrogen.

1.4 Artificial Photocatalytic System Construction.

The goal of the research on artificial photosynthesis is to build a feasible photocatalyst or photocatalytic system capable of converting the energy of sunlight into chemical bonds of hydrogen via the water splitting process. Until now only a few examples of fully operational systems were reported. These systems have been divided in three main categories [11]: i) photoelectrochemical

cells (PECs), ii) suspended nanopowder photocatalysts, and iii) photovoltaic cell-driven electrolyzers.

i) PEC system. [11a]

For water-splitting application, a PEC cell should include two parts, which are a photoanode and a photocathode or a cathode. A photonaode is used to extract electrons from water using the energy of solar irradiation, while a photocathode or a cathode is employed for the hydrogen-generation reaction by using these electrons in reductive processes.

ii) Suspended nanopowder photocatalysts. [11b]

Some semiconductors such as TiO_2 or g-C_3N_4, which have large band gaps, are capable of splitting water into hydrogen and oxygen under UV illumination. In order to enhance their photocatalytic activities, researchers have introduced an oxygen evolution catalyst (OEC) and/or hydrogen evolution catalyst (HEC) on the surface of the semiconductors. These electrocatalysts can function as traps for holes and electrons as well as accelerating the rates of the reactions.

iii) Photovoltaic-electrolyzer combination. [11c]

One promising solution to convert solar energy into electricity is by coupling a solar cell to an electrolyzer, where the electrical energy can be employed for water splitting into hydrogen and oxygen via a classical electrolysis.

In this thesis, density functional theory (DFT) is employed in mechanistic studies of these two important reactions:

1) Catalytic water oxidation using ruthenium based catalysts. In order to design water oxidation catalysts with higher efficiency, a thorough mechanistic understanding for water oxidation is necessary. Recently, a series of mononuclear Ru complexes containing anionic ligand has been synthesized, which show better catalytic activity for water oxidation compared to the catalysts with neutral ligands. With a comparative study of a suite of complexes (Ru-based catalysts bearing anionic and neutral ligands, respectively) we aim to provide an explanation for the promoting effects from anionic ligand and a full mechanistic picture on water oxidation using these catalysts.

2) Proton transfer and H_2 activation/production in iron complexes. Hydrogenases are enzymes that are capable of catalyzing the reversible interconversion between hydrogen and protons efficiently. Inspired by these natural examples, the design of synthetic electrocatalysts for hydrogen oxidation or hydrogen generation has been a goal sought for decades. Computational studies

on these biomimetic iron-based catalysts are needed for a detailed understanding of the mechanisms. One of the most important aspects is the proton transfer or movement in the complex, which is a vital part of the hydrogen generation and uptake. A thorough understanding of the mechanism of proton transfer or movement could serve as a guideline for designing new catalysts for proton reduction. A full mechanistic on hydrogen oxidation using iron-based catalyst has been carried out in this thesis as well.

This thesis is organized in the following manner:

A brief introduction of the mechanism of natural and artificial photosynthesis is given in this chapter as well as the purpose of our research.

A description of theoretical background (redox potential calculation, transition state theory and pK_a calculation) and the adopted methodology (B3LYP and M06) in our calculations (chapter 2).

An introduction to water oxidation catalysts (WOCs based on Ru, Ir, Co and so on) and relevant basic concepts (A hydrogen bonding network effect and OO bond formation) is given in chapter 3.

A description about proton transfer and H_2 activation/generation in natural and synthetic complexes is presented in chapter 4, accompanied with an explanation about the pendant base effect in iron complexes.

A summary of included papers is presented at the end of this thesis.

Chapter 2

Theoretical Background

2.1 A Brief Introduction to Quantum Chemistry

Quantum chemistry is usually considered as one of the subfields of theoretical chemistry. It aims to calculate the various structures and properties of molecules, such as geometry, electronic energy, charge distribution, electric dipole moment, vibrational frequency, etc. by using the principles of theoretical chemistry and the tools of computer science. It aims at explaining the chemical problems specifically.[12]

Since we focus on investigating chemical reactions, which include bond-forming and bond-breaking via transition states, a good description of the electronic distribution is necessary. Usually, quantum chemical methods, which are electronic structure methods ranging from ab initio to semi-empirical methods, are used to calculate the corresponding molecular properties. The ab initio methods only use physical constants and in principle do not need empirical parameters. These methods are constructed so that they, in principle, can be arbitrarily accurate, however, the computational cost increases dramatically to get accurate results for large systems. On the contrary, semi-empirical methods reduce the computational demand for calculation of large systems, however, they are also less general since they are fitted to certain systems.

The time-independent Schrödinger equation [13,14] is shown in Eq. 2-1.

$$H\Psi = E\Psi \tag{2-1}$$

Ψ is the wave function, which determines the given physical system, **H** is the

Hamiltonian operator, which includes kinetic and potential energy, and **E** is the energy of the given system obtained as an eigenvalue to the Hamiltonian.

The Hamiltonian of the time-independent Schrödinger equation within the non-relativistic approximation can be expressed as in Eq. 2-2,

$$\mathrm{H}_{tot} = \mathrm{T}_n + \mathrm{H}_e \tag{2-2}$$

where $\mathrm{T}_n = \sum_a -\frac{1}{2M_a}\nabla_a^2 \qquad \mathrm{H}_e = \mathrm{T}_e + V_{ne} + V_{ee} + V_{nn}$

where **$\mathbf{T_n}$** is the nuclear kinetic energy, **$\mathbf{H_e}$** is the electronic Hamiltonian operator, **$\mathbf{T_e}$** means the electron kinetic energy, **$\mathbf{V_{ne}}$** denotes the attraction between nuclei and electron, **$\mathbf{V_{ee}}$** is the electron-electron repulsion and **$\mathbf{V_{nn}}$** is the nuclei-nuclei repulsion.

Employment of the Born-Oppenheimer approximation further reduces the computational cost of solving the time-independent Schrödinger equation. In this approximation the coupling interaction between the nuclei and electrons is neglected. The electronic part of the Schrödinger equation is solved with the nuclear positions as parameters. The potential energy surface, which results from electronic part solution, is used as a basis to solve the nuclear movement. Hence, for a given set of nuclear coordinates, the large part of the computational cost will lie on the electronic Schrödinger equation solution (Eq. 2-3).

$$\mathrm{H}_e = \mathrm{T}_e + V_{ne} + V_{ee} + V_{nn} \tag{2-3}$$

where $\mathrm{T}_e = \sum_a -\frac{1}{2}\nabla_a^2 \qquad V_{ne} = -\sum_a^{N_{elec}} \sum_i^{N_{elec}} \frac{Z_a}{|R_a - r_i|}$

$$V_{ee} = \sum_i^{N_{elec}} \sum_{j>i}^{N_{elec}} \frac{1}{|r_i - r_j|} \qquad V_{nn} = \sum_a^{N_{elec}} \sum_{b>a}^{N_{elec}} \frac{Z_a Z_b}{|R_a - R_b|}$$

The fundamental methodologies for investigating the properties of a system are divided into two main categories: wave-function based methods and electron density based methods, depending on the different bases.

2.2 Wave-Function Based Methods

Although we have adopted the Born-Oppenheimer approximation to solve the time-independent Schrödinger equation, the electronic Schrödinger equation is still too complicated to solve, since the interactions between all electrons need to be considered.

In Hartree-Fock theory,[15] which takes the interaction between the electrons as an average, the electrons are assumed to move independently under a mean potential field generated by the remaining electrons. Their movements can be written as spin-orbital wave functions separately, and an expression of all the occupied spin-orbital wave functions can be defined as the total electronic wave function for the system. The Hartree-Fock theory includes the exchange interaction between two electrons, which comes from the anti-symmetric property of the wavefunction.

The HF equation can be described as in Eq. 2-4,

$$F\varphi_i = \varepsilon_i \varphi_i \tag{2-4}$$

where $\boldsymbol{F}$ means the Fock operator, $\boldsymbol{\varepsilon_i}$ means the energy of orbital, and $\boldsymbol{\varphi_i}$ the Hartree-Fock molecular orbitals.

The Fock operator includes three terms, and can be expressed as in Eq. 2-5,

$$F = h + \sum_i (J_i - K_i) \tag{2-5}$$

where $\boldsymbol{h}$ denotes the Hamiltonian of a single electron, which includes its kinetic energy and the attraction interaction with the nuclei, and $\boldsymbol{J}$ and $\boldsymbol{K}$ denote the Coulomb operator and exchange operator, respectively.

In general, the Hartree-Fock method cannot give satisfactory accuracy due to the lack of description of correlation interaction, which cannot be captured in a mean field approach. The lack of this correlation interaction always results in a higher energy than the real one. The energy difference between the real energy and HF energy is defined as correlation energy. Although the correlation energy in a system is comparably small, it is often important in relative energies involved in chemical reactions. This correlation interaction should be taken into account especially when calculating reaction barriers.

Therefore, many kinds of more accurate methods based on the Hartree-Fock method are developed to improve the performance, usually referred as post-Hartree-Fock methods such as Configuration Interaction method[16] (CI),

Multi-Configuration Self-Consistent Field method[17] (MCSCF), Many-body Perturbation theory method[18] (MP_n), etc. The correlation energy is considered in different ways with different methods, which improves the results systematically.

The computational cost of those accurate methods is usually huge, especially for large systems, which clearly sets a limitation for broad applications. Fortunately, taken as an improvement in HF method, the Density Functional Theory (DFT) method includes the correlation interaction part, and provides a better balance between computational cost and accuracy. It has therefore become popular in the chemical community in recent years.

2.3 Density Functional Theory (DFT)

As early as 1927, the first attempt of describing the property of a system with electron density was made by Thomas and Fermi. One year later, Dirac added one more term, which described the exchange energy between electrons. Therefore, the Thomas-Fermi-Dirac model is considered a breakthrough in the development of electron density based approaches.[19-21] Different from the wave-function based methods, Density Functional Theory, which is based on the theorems by Hohenberg and Kohn,[22] incorporated the conception of electron density, and the electronic energy of ground state is determined by the electron density entirely. The relationship between the electron density and the energy for a given system is a one to one correspondence.

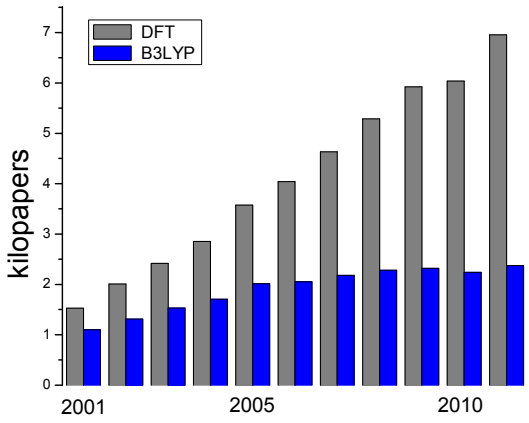

Figure 2.1 *Numbers of papers in Web of Knowledge from 2001 to 2011. (grey bar: "DFT" is searched as a topic; blue bar: B3LYP citations).*

In fact, density functional theory (DFT) has become one of the most popular tools in providing insight into the mechanisms of several vital catalytic cycles in bioinorganic, environmental, and industrial chemistry. The Nobel Prize in

chemistry was awarded to Kohn and Pople in 1998 for their contribution to DFT and computational methods development, respectively.

A general description of its broad application [23] is shown in Figure 2.1.

2.3.1 Hohenberg and Kohn Theorem

Density Functional Theory is based on the proof by Hohenberg and Kohn,[22] a theorem formulated in 1964 that is the basis of Density Functional Theory. The first theorem describes that an external potential v_{ext} is uniquely determined by the electron density, therefore, the total energy of one system, specifically the ground state energy, can be expressed as a functional of the electron density. This theorem states that the electron density determines the properties of a system exclusively. The second theorem describes that we could calculate the electron density of one system by using a variational method, which means we can obtain the true electron density ρ_0 of the system by finding the minimum of the energy functional $E[\rho_0]$.

According to these two theorems, the energy of ground state can be expressed as in Eq. 2-6,

$$E[\rho] = F[\rho] + \int \upsilon_{ext} \rho dr \tag{2-6}$$

Where $\boldsymbol{\rho}$ means the electron density of system, $\boldsymbol{E}$ means the energy of ground state, $\boldsymbol{F}$ means the universal functional composed of electron-electron repulsion energy and electron kinetic energy, and $\boldsymbol{v_{ext}}$ means external potential.

2.3.2 Kohn-Sham Equation

The Hohenberg-Kohn theorems do not describe anything about how the density could be obtained. By solving this problem Kohn-Sham brought back the orbitals to get the density. The expression of Kohn-Sham equation is shown in Eq. 2-7,

$$\left[-\frac{1}{2}\nabla^2 + \upsilon_{eff}(r) \right] \psi_i(r) = \varepsilon_i \psi_i(r) \tag{2-7}$$

$$\upsilon_{eff}(r) = \upsilon(r) + \int \frac{\rho(r')}{|r - r'|} dr' + \upsilon_{xc}(r) \tag{2-8}$$

The first term on the left hand side of Eq. 2-7 is the kinetic energy, $\boldsymbol{\upsilon_{eff}(r)}$ means effective local potential and $\boldsymbol{\upsilon(r)}$ means the external potential, including the

electron-nuclei interaction. The second term on the right hand side of Eq. 2-8 is the electrostatic interaction between electrons, and $v_{xc}(r)$ denotes the exchange-correlation potential.

The exchange-correlation (XC) energy is approximated in practical calculations. Different types of approximations have been introduced into this exchange-correlation term, therefore, many different density functional methods have been proposed and developed.

The simplest exchange-correlation energy approximation is the local density approximation (LDA),[24] which was popular in the 1970s and 1980s. Generalized gradient approximations (GGAs)[25] was introduced in the late 1980s, and it can be used well in chemical reactions with an acceptable accuracy. The currently most popular approximation in chemistry B3LYP was introduced by Becke in the early 1990s. He adopted the Hartree-Fock (HF) exchange instead of a fraction of GGA exchange. Recently, the Minnesota density functionals, especially the M06 family of functionals, were developed by Truhlar's group, and it shows a broad accuracy in many research fields.

2.3.3 Hybrid DFT Method-B3LYP.

There are many DFT methods available at present, where the difference between them lies on the difference choice of functional form related to the exchange and correlation energy. B3LYP as one of the hybrid DFT methods has become very popular, due to its reliable performance.

The exchange-correlation term of B3LYP[26,27] is shown in Eq. 2-9,

$$E_{xc}^{B3LYP} = aE_x^{HF} + (1-a)E_x^{Slater} + bE_x^{B88} + (1-c)E_c^{VWN} + cE_c^{LYP} \qquad (2\text{-}9)$$

For the exchange part, it introduces exact Hartree-Fock exchange in the functional, Slater local functional and Becke 1988 nonlocal gradient correction. For the correlation it includes the Vosko-Wilk-Nusair (VWN) local functional, and the Lee-Yang-Parr local and nonlocal functional.

We have found that density functional theory (DFT) gives highly accurate results, and it can be used for the mechanistic studies in our projects. We adopted B3LYP and M06 to study the mechanism of our target reactions, namely water oxidation and proton reduction.

2.3.3.1 Accuracy on Geometries

The errors in the calculation of geometrical parameters were analyzed by Charles

W. Bauschlicher Jr,[28] standard G2 are used as the benchmark, and consists of 55 molecules containing first and second row atoms. A series of 55 molecules including 71 bond lengths, 26 bond angles and 2 dihedral angles is tested for this purpose.

As shown in Table 2.1, comparing to other approaches the hybrid B3LYP functional has the lowest average error (0.013) when applied to the calculation of bond lengths. The error for B3LYP functional could be further reduced by using a large basis set.

The average absolute deviation on bond angles displays a similar trend, the hybrid functional B3LYP has the smallest error (0.62). Improving the basis set can slightly decrease the error (0.61) at the B3LYP level.

Table 2.1 *The average absolute deviation for geometrical parameters*.

	Bond length (Å) (average absolute error)	Angle (deg) (average absolute error)	Dihedral angle (deg) (average absolute error)
HF[a]	0.020	1.16	1.92
MP2[a]	0.015	0.67	1.24
BLYP[a]	0.026	1.03	0.89
BP[a]	0.020	0.91	0.27
BP86[a]	0.022	0.96	0.24
B3P86[a]	0.010	0.62	0.86
B3LYP[a]	**0.013**	**0.62**	**0.35**
B3LYP (big)[b]	0.008	0.61	3.66

[a] *The 6-31G* basis set is used*

[b] *The 6-311 + G(3df, 2p) basis set is used*

Different from the bond angles and bond lengths, B3LYP does not have the smallest error when calculating dihedral angles, however, it is acceptable. Since the analysis only includes two dihedral angles, it is not likely to accurately describe the reliability of dihedral calculation using the approaches mentioned above.

2.3.3.2 Accuracy on Energies

In order to test the B3LYP accuracy on various energy calculations, which includes atomization energy, electron affinity, barrier height, etc., many reports have been published by various groups. One of them is the atomization energy calculations reported by Charles W. Bauschlicher Jr.

Table 2.2 *The average absolute deviation for atomization energy calculation.*

	Atomization energy (kcal/mol) (average absolute error) [a]	Atomization energy (kcal/mol) (average absolute error) [b]
HF	80.52	74.50
MP2	16.04	7.43
BP	8.21	11.81
BLYP	5.31	4.95
BP86	7.23	10.32
B3P86	5.87	7.82
B3LYP	**5.18**	**2.20**

[a] *The 6-31G* basis set is used*

[b] *The 6-311 + G(3df, 2p) basis set is used*

From Table 2.2, it is clear that the hybrid functional B3LYP demonstrates superior performance over other approaches. The average absolute error is 5.18 kcal/mol using a small basis set. Improving the basis set lead to a decrease to 2.2 kcal/mol.

In 2005 a new extensive set [29] based on G3/05 containing a total of 454 energies was used to test for validation of quantum chemical methods. After comparison, B3LYP still stands out of other approaches within a mean unsigned error of 4.14 kcal/mol. Furthermore, the results indicate that B3LYP performs as well or even better than B98, which is considered as the most accurate functional in this G3/05 test set for smaller molecules.

2.3.4 Recently Developed Hybrid DFT Methods

Recently, many new approximate density functionals in the framework of Kohn-Sham density functional theory have been developed to improve the performance of DFT, such as the Minnesota density functionals, density functional theory including dispersion corrections, etc. These improved DFT methods aim at meeting two fundamental conditions required by a good density functional approach. Firstly, they can produce a high accuracy for basic physical and chemical properties, such as geometry and energy. Secondly, these improved methods can be applied to a general research field (including organometallic chemistry, inorganic and organic chemistry, and biochemistry) and provide a good description.

2.3.4.1 The Minnesota Density Functionals

The Truhlar group has developed several approximate functionals, named the

Minnesota density functionals, which are a series of approximated exchange-correlation energy functionals in DFT. One of them is the M06 family,[30] including the functionals M06-L, M06, M06-HF and M06-2X, and the difference among those functionals is mainly the different amount of exact HF exchange . These functionals show successful applications in many fields, such as organometallic, inorganic, organic and biological chemistry. Compared to B3LYP, the M06 family shows a better performance for organic chemistry due to the improved treatment of medium-range correlation energy. We have chosen this method to give a more accurate electronic energy in our system.

Ten functionals were tested by the Truhlar group against the dissociation energies of four 16T-isobutene complexes (four possible models of the dissociation of isobutene from 16T zeolite model cluster).[31] Two of them (π-complex and *tert*-butyl carbenium ion) are non-covalent, while the other (*tert*-butoxide and isotutoxide) two are covalent. The results (Table 2.3) showed that, M05-2X and M06-2X gave the best performance, followed by M06-L and M06. All these four functionals gave a small MAD value. However, the other six functionals did not give an acceptable result. The M06 family produces a satisfactory result for both covalent and non-covalent cases.

Table 2.3 *A benchmark data of dissociation energies (kcal/mol) in four complexes involving the dissociation of isobutene from a 16T Zeolite cluster model.*

	π-complex (non-covalent)	*tert*-butyl carbenium ion (non-covalent)	*tert*-butoxide (covalent)	isotutoxide (covalent)	mean error
method[a]	D_e-C_p	D_e-C_p	D_e-C_p	D_e-C_p	MAD-C_p
Best estimate	15.1	-9.8	13.9	13.9	
M05-2X	**11.7**	**-8.1**	**14.9**	**14.0**	**1.6**
M06-2X	**12.7**	**-9.1**	**16.6**	**15.6**	**1.9**
M06-L	**14.4**	**-2.3**	**15.6**	**13.5**	**2.6**
M06	**13.3**	**-3.9**	**16.0**	**14.4**	**2.6**
M06-HF	12.4	-12.5	18.6	18.8	3.7
PBEh	2.9	-15.6	4.7	4.7	9.1
PBE	3.2	-12.8	2.3	2.0	9.6
B97-1	3.9	-14.3	2.2	2.9	9.6
TPSSh	-0.9	-17.7	1.8	1.6	12.1
B3LYP	-2.5	-20.7	-5.5	-4.8	16.6

[a] *The 6-311+G (2df, 2p) basis set is used for all density functionals in this table. MAD denotes mean absolute deviation, and D_e-C_p denotes dissociation energy calculation with counterpoise correction*

2.3.4.2 Density Functional Theory Including Dispersion Corrections

Non-covalent interactions, such as the attractive long-range van der Waals (dispersion) interactions, plays an increasingly vital role in the theoretical description of chemical research, especially in organic chemistry, supramolecular chemistry and biochemistry. Several density functional approximations have been developed to include this weak interaction. Density functional Theory- Dispersion (DFT-D) uses a dispersion correction term, which is an empirical correction based on a classical London dispersion description of the interaction based on atom pairs, in Kohn-Sham density functional theory. It has been applied successfully in various fields of chemistry.

The common G3/99 set of heat of formation (HOF) is adopted by the Grimme group to test the general applicability.[33] The G3/99 set includes relatively large molecules, therefore, intramolecular dispersion makes a significant contribution. Three density functionals (B3LYP, B2PLYP and mPW2PLYP) with and without the dispersion correction were adopted for comparison. The results with the dispersion correction improved remarkably for all three functionals. A statistical summary of their results is shown in Table 2.4.

Table 2.4 *Performance of three functionals (B3LYP, B2PLYP and mPW2PLYP) with and without the dispersion corrections. All values are in kcal/mol.*

Functional	MD[a]	MAD[b]
B3LYP	-4.6	5.6
B3LYP-D	**-1.3**	**3.1**
B2PLYP	-1.7	2.4
B2PLYP-D	**0.0**	**1.7**
mPW2PLYP	-1.4	2.1
mPW2PLYP-D	**-0.2**	**1.7**

[a] *MD means the Mean Deviation.*

[b] *MAD means the Mean Absolute Deviation.*

2.4 Redox Potential Calculations

Accurate prediction of redox potentials of transition metal complexes, which has

drawn much attention over the past several years, is highly desirable in electrochemistry. A computational approach using DFT to finding a redox potential within a specific range is available for a long time. DFT has been used to facilitate in the rational design of catalysts with this specific property (redox potentials).

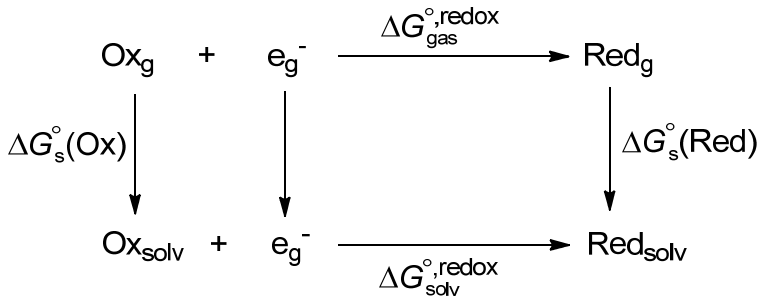

Scheme 2.1 *Born-Haber Cycle.*

Currently there are several protocols available for the computational prediction of the standard redox potentials in solution.[34] One of the most popular methods is by using the Born-Haber cycle. (Scheme 2.1)

The overall reaction of the standard Gibbs free energy ΔG_{solv} redox (kcal/mol) is calculated as Eq. 2-10.

$$\Delta G^{\circ,redox}_{solv} = \Delta G^{\circ,redox}_{gas} + \Delta G^{\circ}_s(Red) - \Delta G^{\circ}_s(Ox) \quad (2\text{-}10)$$

The first term on the left hand side of Eq. 2-10 is the free energy change in the solvent. The terms on the right hand side are the free energy change in the gas phase, the solvation free energies of the reduced and oxidized species, respectively.

And the Nernst equation (Eq. 2-11) determines the standard one electron redox potentials, E/V.

$$\Delta G^{\circ,redox}_{solv} = -FE^{\circ}_{calc} \quad (2\text{-}11)$$

where F is the Faraday constant, 23.06 kcal·mol^{-1} V^{-1}.

2.5 Transition State Theory

Transition state theory, which was developed by Eyring and coworkers in 1935,[35] has been proven to be a considerable success in the application of a wide variety of processes. This theory is generally used to calculate the reaction rates of chemical reactions, and describe qualitatively how a chemical reaction occurs,

especially important for catalytic reactions.

As reactant **A** is converting to product **B** in the reaction, a bond breaking and a new bond forming are often involved. The transition state forms or activated complex **A*** are usually assumed to exist as intermediate states during the reaction. (Figure 2.2).

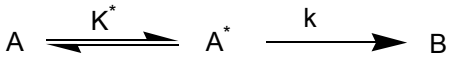

Figure 2.2

The rate constant *k* of a reaction can be described as follows (Eq. 2-12),

$$k = \frac{k_B T}{h} e^{\frac{-\Delta G^{\neq}}{RT}} \tag{2-12}$$

where k_B denotes the Boltzmann's constant (1.38×10^{-23} J/K), h is Plank's constant (6.63×10^{-34} J s), $\Delta G^{\neq}$ is the difference in Gibbs free energy between reactant and the transition state, R is the gas constant (8.314 J K^{-1} mol^{-1}), and T is the temperature in Kelvin.

From the formula above, we can derive that a rate of 1 s^{-1}, which indicates one unit of reaction per second, corresponds to a barrier of 17.4 kcal/mol at room temperature (298.15K). A change of 1.4 kcal/mol in activation barrier depicts an approximate raise or fall in reaction rate by one order of magnitude. These useful relationships can serve as a guideline for our mechanistic research, and help us assess the feasibilities of related reaction and compare different mechanistic proposals.

2.6 pK_a Calculation

The Gibbs free energy change of deprotonation of HA in water $\Delta G^{o}_{deprot,\ aq}$ (Scheme 2.2) is defined as Eq. 2-13.

$$\Delta G^{\circ}_{deprot,\ aq} = \Delta G^{\circ}_{aq}(A^-) + \Delta G^{\circ}_{aq}(H^+) - \Delta G^{\circ}_{aq}(HA) \tag{2-13}$$

In water the standard free energy of species (A^-, H^+ and HA) ΔG^{o}_{aq} can be calculated by adding the standard free energy in gas phase ΔG^{o}_{g} and the standard free energy of solvation in water ΔG^{o}_{solv} together (Eq. 2-14),

$$\Delta G^{\circ}_{aq} = \Delta G^{\circ}_{g} + \Delta G^{\circ}_{solv} \tag{2-14}$$

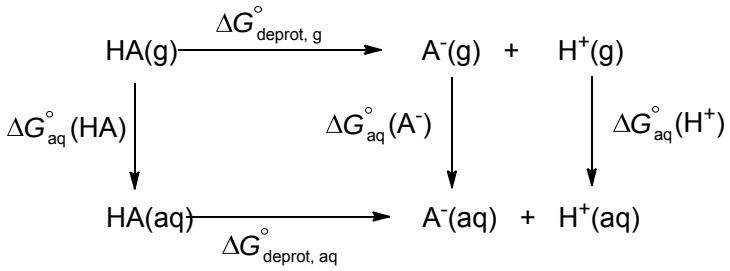

Scheme 2.2 *The calculation of a pK_a value using thermodynamic cycle.*

The calculation of the pK_a value of an acid HA in aqueous solution [36] is related to the Gibbs free energy change of the deprotonation process $\Delta G^{o}_{deprot,\ aq}$ (Eq. 2-15). And it can be expressed as

$$pK_a = \frac{1}{2.303RT} \Delta G^{\circ}_{deprot,\ aq} \qquad (2\text{-}15)$$

where R is the gas constant (8.314 J K^{-1} mol^{-1}) and T is the temperature in Kelvin.

2.7 Solvation Model

In this thesis, the reactions were carried out in a certain solvent, either in water or in dichloromethane. In order to describe solvated molecular systems we use a self-consistent reaction field method, which means first we solve the Schrödinger equation by selecting an approximate Hamiltonian to get a more accurate set of orbitals, then solve the Schrödinger equation again with and applied field until the self-consistency having been obtained. To consider the solvation effect in our research, the solvation free energies corrections, which is the difference between the energy of optimized geometry in gas phase and the same optimized geometry in a certain solvent, were calculated using Poisson-Boltzmann Solvation Model implemented in Jaguar.[37] Furthermore, to reproduce the strong hydrogen bonding interaction with the solvent precisely the geometries of the Ru-aqua complexes containing O-H bonds were optimized with additional water molecules around them by forming a reasonable hydrogen-bonding network.

2.8 Theoretical Studies

Generally, the theoretical studies in this thesis including water oxidation and proton reduction are based on Density Functional Theory (DFT), and they can in

general be depicted as in our papers[82] "*All calculations were performed with Jaguar 7.6 program package of Schrödinger LLC. Becke's three-parameter hybrid functional and the LYP correlation functional (B3LYP) was employed with the LACVP** core potential and basis set for geometry optimizations, frequency and solvation energy calculations, while the M06 functional using the LACV3P**++ basis set (augmented with two f-polarization functions on M (Fe or Ru) as suggested by Martin[38]) was used for single point energy corrections. In order to confirm whether the geometries correspond to minima or first-order saddle points (transition states) or not on the potential energy surface (PES), frequency calculations were performed using the optimized geometries. The expression for Gibbs free energies were presented as the following equation* $G = E(M06/LACV3P^{**}++ 2f \text{ on } M) + G_{solv} + ZPE + H_{298} - TS_{298} + 1.9$ *(1.9 denotes the concentration correction to the free energy of solvation from 1 M(g)* $\rightarrow$ *1 M(solv) to 1 atm(g)* $\rightarrow$ *1 M(solv)). The solvation model adopted was the Poisson-Boltzmann reactive field (PBF) implemented in Jaguar 7.6. For free energy of solvating proton, we chose the experimental number by Tissandier[39] et al. of* -264 *kcal* mol^{-1} *(for the free energy of 1M proton in water the value of* -270.3 *kcal* mol^{-1} *was adopted)*."

Chapter 3

Experimental and Theoretical Studies on Water Oxidation Catalysts.

3.1 Brief Introduction

Trying to find a sustainable fuel to change our current energy consumption infrastructure is probably one of the greatest challenges facing the world. Searching and building a renewable and sustainable energy source is one of the key points in such a system. Energy from sunlight is considered as an inexhaustible and decentralized resource, and energy produced by one hour of sunlight (4.3×10^{20} J) could satisfy the energy consumption on the planet in one year (4.1×10^{20} J).[40a] The conversion of solar energy into electricity or other forms of energy, which is one of the methods of energy storage, is a very promising way to solve this problem. Energy storage plays a critical role in balancing the supply and demand of energy and therefore securing our energy future. The development of storage technologies is therefore crucial to achieve this target. Generally, energy storage systems [40b] can be categorized into four sectors, which are mechanical, bio-chemical, electrical and thermal forms.

1) Mechanical form. Compressed Air Energy Storage (CAES) system was constructed recently. In the form of compressed air it stores energy in a deep underground geological vessel or reservoir. Electricity from the grid powers compressors is used to drive air into the storage vessel underground during off-peak hours. When peak hours come, the stored air is released and heated with natural gas to expand its velocity. This air-gas mixture then can be used in a combustion turbine which can generate power for use.

2) Bio-Chemical form. Biofuels are gaining increased attention of both the public and scientists recently. This kind of fuel is formed by biological carbon fixation and can be derived from biomass conversion. A considerable amount of solar energy is stored as chemical energy in this process, and the stored energy then can be released in a straightforward way. The widely utilization of biofuels such as bioethanol, biodiesel, biogas, etc., would increase energy security. This is the class of sunlight-to-bio-chemical energy storage.

3) Electrical form. Many kinds of rechargeable batteries such as Lead-acid, Carbon-zinc, Lithium-ion etc., are usually used to store spare electricity, and the stored electricity can be used at times when a demand comes. As the stored energy in battery is used up, it is easy to recharge.

4) Thermal form. This means the temporary storage of heat or cold for later use, ice-storage for air conditioning on hot summer days is one example, water is frozen into ice at night, when electricity consumption cost is lower, then the cool of the ice can be used in the afternoon to meet conditioning demand as well as reduce the electricity consumption in daytime when cost is higher. This ice storage is produced with a lower electrical utility rate.

Converting electrical energy from sustainable sources to stored chemical energy in the form of fuels is highly desirable. From a more general perspective, fuels are reductants, an abundant and clean source of electrons is therefore required to make them. The most logical source of these electrons is from water, since water is the most abundant molecule on earth. Recently, much effort has been put to convert solar energy into electricity, and the discovery of the new type device showed that low cost materials can be used in the construction of solar cells. Another way to utilize solar energy is water splitting with production of molecular oxygen and hydrogen.[41]

The function of Photosynthesis provides an almost perfect example to solar energy utilization including solar capture, conversion and storage. This process provides energy for nearly all life on the earth. The generation of oxygen [42] from water takes place at an active site in Photosystem II (PS-II). This active center contains four manganese ions, which is a binuclear bis(μ-oxo) dimanganese unit. This cluster containing four manganese ions is named the Oxygen Evolving Complex (OEC).[43,44]

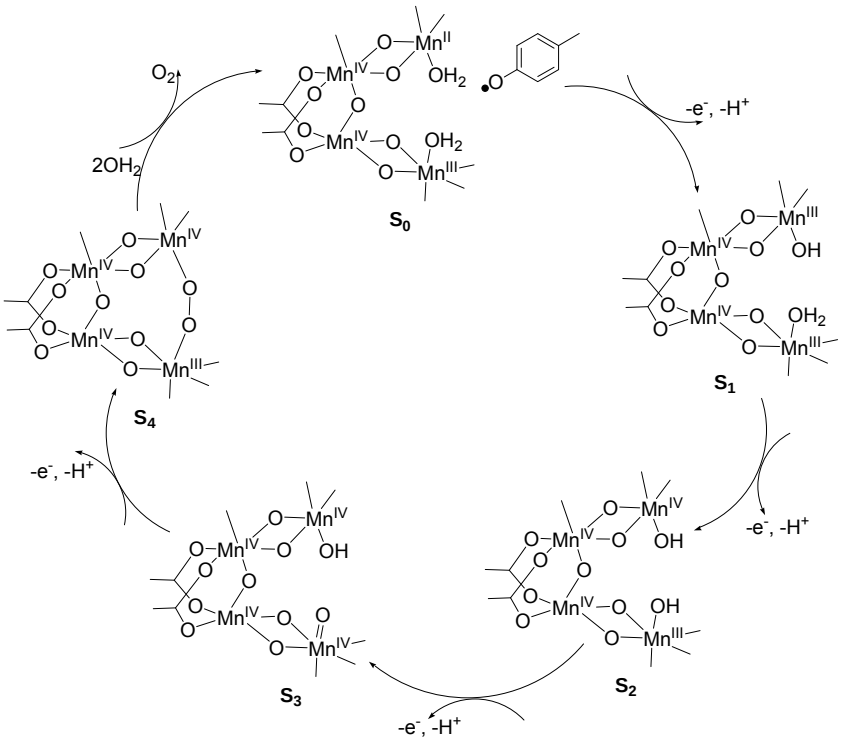

Figure 3.1 *Proposed mechanism on water oxidation at the OEC in photosystem II.*

Many papers reported the possible mechanisms[45] related to oxygen evolution at this active center. One general proposal is show in Figure 3.1. It is recognized that the release of oxygen from water takes place via a stepwise proton-coupled electron transfer, resulting in the manganese complex from the sequentially oxidized state S_0 to S_4. At state S_4, O_2 is generated while two water molecules come in, and finally the complex returns to the state S_0.

Inspired by the function of PS-II, many artificial photosynthesis systems aiming at producing oxygen by light-driven water splitting have recently been built. In order to mimic the function of the oxygen evolving complex (OEC) in PS-II, much effort has been devoted to the development of molecular catalysts in order to be able to oxidize water, and this is identified to be one of the bottlenecks for the application of artificial photosynthesis. The design of qualified water oxidation catalysts [46-54] (WOCs) is one of the keys for an artificial photosynthesis system with high efficiency. However, only a few artificial bio-inspired complexes display a satisfactory performance on catalytic O_2 generation from water. Several series of efficient WOCs based on Ru, Ir, and first row transition metals (Fe, Co, Ni and Cu), have been reported over the last years.

3.2 Introduction to Proton-Coupled Electron Transfer (PCET).

Charge separation is the basis of photosynthetic energy utilization, which is

carried out in biological systems. The electron transfer that occurs in the charge separation is frequently accompanied with proton transfer, such as in Photosystem II (PS-II), and this is called Proton-Coupled Electron Transfer (PCET) reactions.[55,56] The theory on PCET reaction has been developed over several years. It is depicted as[57] *"the nonadiabatic transitions between the reactant and product electron-proton vibronic states"*. Actually, this kind of reaction plays a vital role in a wide range of biological processes, such as respiration and photosynthesis.

In PS II, upon the absorption of a photon, P680 is excited and becomes strongly reducing and transfers an electron to the acceptor and forms $P680^+$. Then a tyrosine group (Tyrz) donates one electron to the $P680^+$, and simultaneously dissociates its phenolic proton to a base nearby.

In order to mimic the proton coupled electron transfer function in PS II, Hammarström and coworkers used a synthetic compound [58,59] to investigate the electron transferring of tyrosine (Figure 3.2). They took ruthenium-tris-bipyridine ($Ru(bpy)_3$) as a photosensitizer, after exposure to a laser flash (λ = 460nm), the $Ru(bpy)_3$ reaches its excited state and loses one electron. The oxidized $Ru(bpy)_3$ can receive one electron from the tyrosine, which transfers one electron and is deprotonated simultaneously.

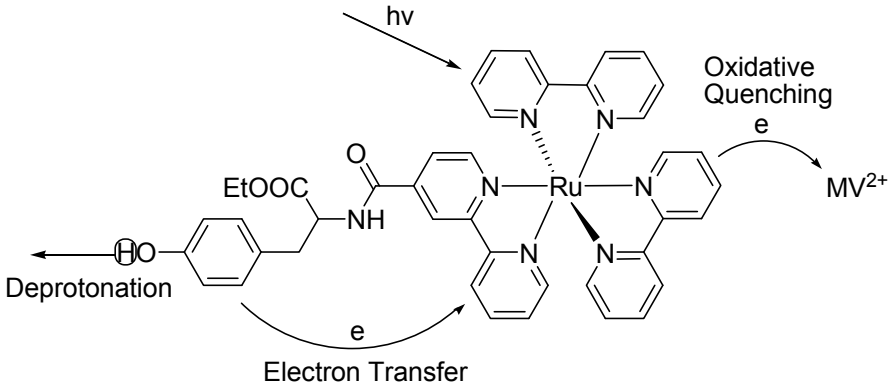

Figure 3.2 *Proton coupled electron transfer from tyrosine. The supramolecular system* $Ru^{II}(bpy)_2$*(4-Me-4'-CONH-L-tyrosine etyl ester-2,2'-bpy)*$^{2+}$.

In fact, PCET processes are important for oxygen evolution in artificial photosynthetic systems as well. Water is required to be oxidized to produce oxygen, however, this is not straight forward. The thermodynamic potentials decrease as the number of electrons transferred increase (Table 3.1).[60,61] The required thermodynamic potential for oxygen evolution from water is 1.23 V vs. NHE at pH 0, and this water oxidation involves the loss of four protons and four

electrons. The designed catalysts should have the property of multiple electron transfer. Therefore, transition metal complexes are considered as suitable candidates to perform this reaction in a catalytic manner since they often have many accessible oxidation states. Among them, ruthenium aqua complexes meet these requirements, since the Ru complexes has the ability of losing protons and electrons to reach their higher oxidation states.

Table 3.1

Redox couple	E, V (vs. NHE)
$\bullet OH + 1H^+ + 1e^- — H_2O$	2.81
$HO\text{-}OH + 2H^+ + 2e^- — 2H_2O$	1.78
$HOO\bullet + 3H^+ + 3e^- — 2H_2O$	1.51
$O=O + 4H^+ + 4e^- — 2H_2O$	1.23

(a) *cis*-$[Ru^{II}(bpy)_2(py)(H_2O)]^{2+} \xrightarrow{0.67\ V}$ *cis*-$[Ru^{III}(bpy)_2(py)(OH)]^{2+} \xrightarrow{0.78\ V}$ *cis*-$[Ru^{IV}(bpy)_2(py)(O)]^{2+}$

V vs NHE, u=0.1M, pH=7

(b) *cis*-$[Ru^{II}(bpy)_2(Cl)_2]^0 \xrightarrow{0.0\ V}$ *cis*-$[Ru^{III}(bpy)_2(Cl)_2]^{1+} \xrightarrow{1.7\ V}$ *cis*-$[Ru^{IV}(bpy)_2(Cl)_2]^{2+}$

V vs NHE, 0.1M $[N(n\text{-}Bu_4)PF_6/CH_3CN]$

Scheme 3.2 *Oxidation potentials for two sets of ruthenium polypyridyl based redox couples.*

Without involving high energy intermediates PCET provides a plausible reaction pathway to access the higher states for ruthenium aqua complexes.[62-64] The comparison in Scheme 3.2 provides an explanation for the advantage of ruthenium aqua complex. The redox potential difference between Ru(IV/III) and Ru(III/II) is only 0.11V for ruthenium aqua complex (Scheme 3.2 a), while this difference jumps to 1.7V for ruthenium chloride complex (Scheme 3.2 b). The smaller difference in oxidation of the ruthenium aqua complex indicates that the coordination of water stabilizes Ru(IV) dramatically. The main reason for this stabilization of higher oxidation state is the oxo formation. It also indicates that the conditions required for oxidation from Ru(II) to Ru(IV) are relatively mild for ruthenium aqua complexes.

One specific example[65] of PCET is the “blue dimer”. The initial oxidation state $H_2O\text{-}Ru^{III}\text{-}O\text{-}Ru^{III}\text{-}OH_2$ also undergoes oxidative activation via proton-coupled electron transfer pathways, which means a simultaneous loss of protons and electron occurs. PCET is important for the blue dimer to build up multiple oxidative equivalents without increasing positive charge.

3.3 Water Oxidation Catalysts

3.3.1 Ruthenium-Based WOCs.

3.3.1.1 Dimeric Ruthenium-Based WOC.

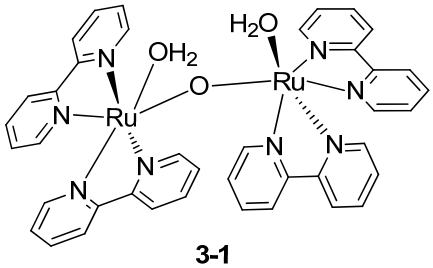

3-1

(13, 0.004 s^{-1})

Figure 3.3 *Structure of cis,cis-[(bpy)$_2$(H$_2$O)Ru^{III}-O-Ru^{III}-(H$_2$O)(bpy)$_2$]$^{4+}$. TON and TOF values are given in parentheses, respectively.*

Complex **3-1** *cis,cis*-[(bpy)$_2$(H$_2$O)Ru^{III}-O-Ru^{III}-(H$_2$O)(bpy)$_2$]$^{4+}$ (bpy = bipyridine) normally referred to as the blue dimer[66] due to its deep blue color, was first reported by Meyer's group. The feature of this dimer is two Ru-OH$_2$ units are connected by a dianionic oxido ligand (Figure 3.3), which results in an electronic coupling between the two metal centers, and therefore shows interesting electrochemical properties, such as redox behaviors and its catalytic properties by extension.

The X-ray structure [67] of this blue dimer is shown in Figure 3.4:

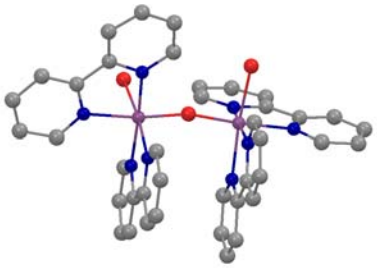

Figure 3.4 *X-ray structure of complex **3-1** cis,cis-[(bpy)$_2$(H$_2$O)Ru^{III}-O-Ru^{III}-(H$_2$O)(bpy)$_2$]$^{4+}$. Hydrogen atoms are omitted for clarity. (purple for Ru, grey for C, red for O and blue for N).*

When adding Ce^{IV} into the acidic solutions containing the blue dimer, gas is released from the solution. After gas chromatographic and mass spectrometric

measurements, the released gas was confirmed to be oxygen. The turnover number (TON) is around 13 and the turnover frequency (TOF) is 0.004 s^{-1}. This ruthenium complex was taken as a landmark in water splitting since it is the first synthetic molecular catalyst for water oxidation. The mechanistic and kinetic studies of Ce^{IV} oxidation of this blue dimer will be discussed in detail later in this chapter.

The first water oxidation catalyst 'blue dimer' carries a dimeric structure, and the two Ru fragments are connected via an oxo bridge that tends to cleave, which limits the lifetime of the catalysts. The discussion about the requirement for dimeric or higher order structures was in debate until the discovery of monomeric ruthenium-based WOCs.

3.3.1.2 Monomeric Ruthenium-Based WOCs Carrying Neutral Ligands.

Several monomeric complexes based on Ru were presented by Thummel's group.[68-70] These complexes also displayed a good performance on catalytic water oxidation. This demonstrated that one site is enough for catalytic water oxidation. In fact, the discovery of mononuclear ruthenium WOCs is one of the major recent breakthroughs.

In 2005, the hydrogen-bonded aqua complex **3-2** *trans*-$[Ru(pbn)(4\text{-R-py})_2(OH_2)]^{2+}$ (pbn = 2,2'-[4-(tert-butyl)pyridine-2,6-diyl]bis(1,8-naphthyridine); py = pyridine)[71] (Figure 3.5), which contains only one Ru center was reported by Thummel's group. It was encouraging that this mononuclear catalyst also could perform water oxidation, which provides a qualitative evidence for catalytic activity of mono-nuclear catalyst.

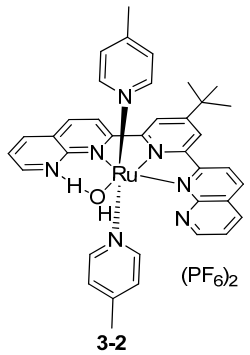

3-2

(260, 0.014 s^{-1})

Figure 3.5 *Structure of complex **3-2**, trans-$[Ru(pbn)(4\text{-Me-py})_2(OH_2)]^{2+}$. TON and TOF values are given in parentheses, respectively.*

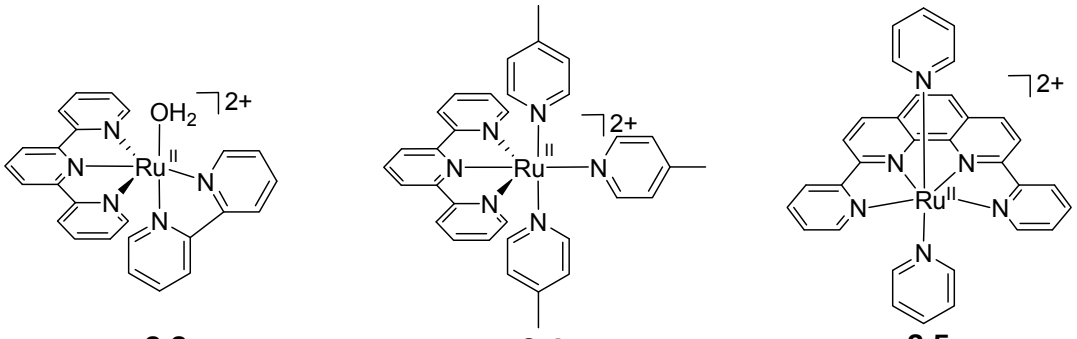

3-3 (310, 0.029 s^{-1}) **3-4** (89, ---) **3-5** (416, 0.028 s^{-1})

Figure 3.6 *Molecular structures of mono-nuclear Ru (II) catalysts. TON and TOF values are given in parentheses, respectively.*

Afterwards, a series of monomeric ruthenium WOCs were synthesized, as shown in Figure 3.6. All those complexes, **3-3** $Ru(tpy)(bpy)OH_2$ (tpy = terpyridine; bpy = bipyridine), **3-4** $Ru(tpy)(pic)_3$ (pic = 4-picoline) and **3-5** $Ru(dpp)(py)_2$ (dpp = 2,9-dipyrid-2'-yl-1,10-phenanthroline; py = pyridine) are active catalysts for water oxidation, although their activities are different between different series.

3.3.1.3 Monomeric Ruthenium-Based WOCs Carrying Anionic Ligands .

Recent research shows that the introduction of anionic (negatively charged) ligands,[72-75] as in complexes **3-6** $Ru(bda)(pic)_2$ (H_2bda = 2,2'-bipyridine-6,6'-dicarboxylic acid; pic = 4-picoline) and **3-7** $Ru(bda)(isoq)_2$ (isoq = isoquinoline)**,** and **3-8** $Ru(pdc)(pic)_3$ (H_2pdc = 2,6-pyridine-dicarboxylic acid; pic = 4-picoline.) (Figure 3.7), yields significantly improved catalytic activity compared to complexes bearing neutral ligands. This is because the introduction of negatively charged ligands results in destabilization of the filled d orbitals of ruthenium complexes with lower-valence, due to d_π-p_π repulsion. When the ruthenium complexes reach high-valent states, these negatively charged ligands provide stabilization by favourable interaction between the empty d-orbitals of the ruthenium and filled p-orbitals of the oxygen atoms.

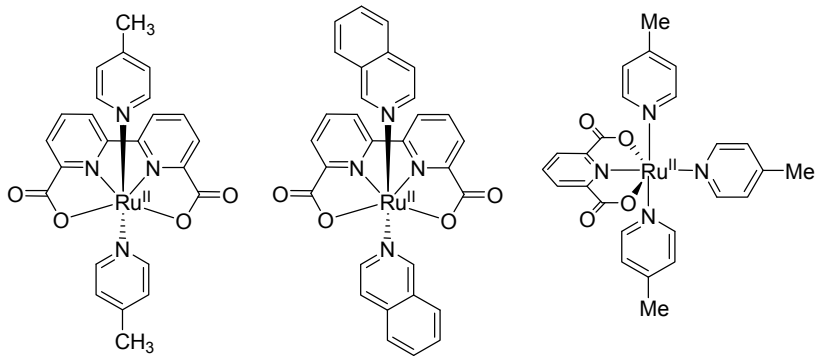

3-6 (2000, 18 s^{-1}) **3-7** (8440, 469 s^{-1}) **3-8** (550, 0.23 s^{-1})

Figure 3.7 *Molecular structures of complexes **3-6, 3-7, 3-8**. TON and TOF values are given in parentheses, respectively.*

3.3.2 Iridium-Based WOCs

Several complexes based on iridium display water oxidation activity. The cyclometalated iridium-based complex **3-9** $[Ir(5\text{-}F,4'\text{-}F\text{-}phenylpyridine)_2(OH_2)_2]^+$ has been synthesized by Bernhard's group.[76]

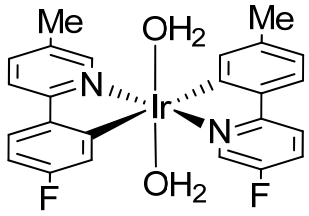

3-9 (2760, 0.004 s^{-1})

Figure 3.8 *Molecular structure of $[Ir(5\text{-}F,4'\text{-}F\text{-}phenylpyridine)_2(OH_2)_2]^+$. TON and TOF values are given in parentheses, respectively.*

This kind of water oxidation catalyst (Figure 3.8) shows some impressive properties, such as robustness, high-efficiency, and easy-modification. However, the low catalytic rate limits its broad application. Usually it requires long times (around one week) to complete the reaction.

Just recently one exceptional water oxidation catalyst $[Cp^*Ir^{III}(NHC)Cl_2]$ (in which NHC=3-methyl-1-(1-phenylethyl)-im-idazoline-2-ylidene) has been found by the Lloret Fillol group (Figure 3.9), complex **3-10** shows an extraordinarily high catalytic activity towards homogeneous water oxidation when employing

$NaIO_4$ as a sacrificial oxidant, with a TON of 400 000 and long-term TOF of 9000 h^{-1}. [77]

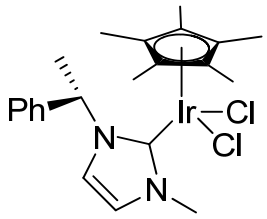

3-10

(400000, 9000 h^{-1})

Figure 3.9 *Molecular structure of [Cp*Ir^{III}(NHC)Cl$_2$]. TON and TOF values are given in parentheses, respectively.*

Furthermore, it shows no noticeable degradation of the activity to water oxidation, even after a several-month storage of reaction solutions. This is susceptible to be applied to long-lasting electrochemical cells.

3.3.3 First-Row Transition Metal Based WOCs

Artificial water oxidation catalysts using first row transition metals such as manganese, iron, and cobalt, are recently gained attention. More groups are concentrating on the development of water oxidation catalysts based on abundant, inexpensive metals, such as those of the first transition metal series.

3.3.3.1 Manganese-Based WOCs

Synthetic water oxidation catalysts based on manganese have come into notice since complex **3-11** $[(tpy)(H_2O)Mn(\mu\text{-}O)_2Mn(tpy)(H_2O)]^{3+}$ (tpy = 2,2':6',2''-terpyridine) (Figure 3.10) was reported by Brudvig's group.[78] The TON reaches a moderate number of 17 using Ce^{IV} as an oxidant.

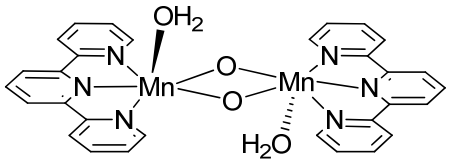

3-11

(17, ---)

Figure 3.10 *Molecular structure of* complex **3-11** *[(tpy)(H$_2$O)Mn(μ-O)$_2$Mn(tpy)(H$_2$O)]$^{3+}$, TON and TOF values are given in parentheses, respectively.*

3.3.3.2 Cobalt-Based WOCs

Complex **3-12** Cobalt-based β–octa-fluoro hangman corrole was reported by Nocera's group in 2011.[79a] It contains *meso*-pentafluorophenyl and β–octa-fluoro substituents (Figure 3.11), and shows a satisfactory performance on water oxidation. This complex is confirmed as one of the most active catalysts among cobalt corroles.

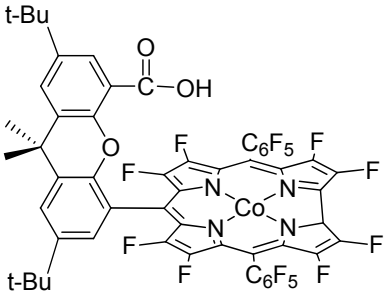

3-12

(---, 1 s^{-1})

Figure 3.11 *Molecular structure of cobalt-based β–octa-fluoro hangman corrole. TON and TOF values are given in parentheses, respectively.*

The TOFs per Co atom for **3-12** can approach around 1 s^{-1} (at pH 7) when immobilized in Nafion films, which is higher than other cobalt-based water oxidation complexes.

3.3.3.3 Iron-Based WOCs

The iron-based catalysts for homogeneous water oxidation is attractive since the metal is abundant, inexpensive and environmentally benign [79b]. The iron complex **3-13** [Fe(OTf)2(mcp)] bearing tetradentate nitrogen ligands (mcp = N,N′ -dimethyl-N,N′ -bis(2-pyridylmethyl)-cyclohexane-1,2-diamine, OTf = $CF_3SO_3^-$) was found to be highly active by the Lloret Fillol group. This complex is environmentally benign, and shows an efficient performance on catalyzing homogeneous water oxidation during several hours [79c,79d]. Turnover numbers >1000 and >350 were attained using sodium periodate at pH 2 and cerium ammonium nitrate (CAN) at pH 1 (Figure 3.12).

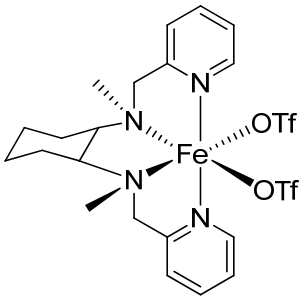

3-13

(1050, 222, $NaIO_4$; 360, 838, CAN)

Figure 3.12 *Molecular structure of complex **3-13** [Fe(OTf)$_2$(mcp)], TON and TOF values are given in parentheses using sodium periodate and cerium ammonium nitrate as sacrificial oxidants, respectively.*

To date, the number of catalytic cycles per metal center, which is more than 1000, obtained by this iron catalyst is the highest reported for any homogeneous system based on 1st-row transition metals.

3.3.3.4 Copper-Based WOCs

Complex **3-14** (2, 2'-bipyridine)Cu(OH)$_2$ is the first copper-based catalyst for the electrolytic homogeneous water oxidation, [80a] this opens a new window in water oxidation catalyst design using the earth-abundant and inexpensive metal. Furthermore, copper complexes are attractive targets for water oxidation because of their extensive biomimetic chemistry with O_2. [80b, 80c, 80d]

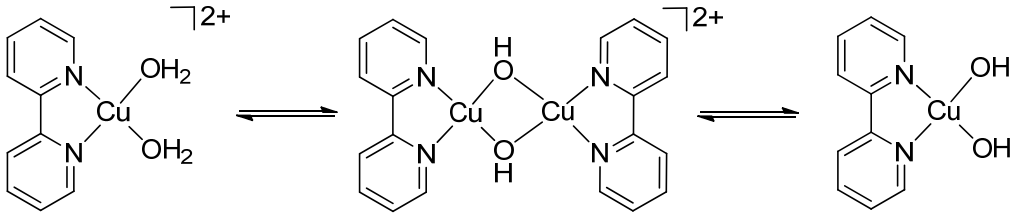

3-14

(---, 100 s^{-1})

Figure 3.13 *The aqueous speciation of a 1:1 copper(II):bpy solution.*

This copper-bipyridine catalyst is described as self-assembling from simple bipyridine and copper salts in aqueous solution at the appropriate basic pH, and large catalytic currents are observed when solution contains substantial amounts of (bpy)Cu(OH)$_2$ (Figure 3.13).

3.4 A Hydrogen-Bonding Network Effect

Hydrogen bonds which are involving multiple peptide carbonyl groups to water form a network around the oxygen-evolving complex (OEC) in photosystem II. Some research results demonstrate that this hydrogen bonding network could be involved in the catalytic water oxidation and play a key role in this process.

The position of bound water molecules has been confirmed by the Kamiya research group.[81a] There are approximately 1300 water molecules per monomer of PS-II, four water molecules are proposed to be placed at the active reaction center OEC. Two of them were predicted to bind to manganese, and another two waters are bound to calcium (Figure 3.14). This structure confirmation suggests that at the OEC water forms wide hydrogen-bonding network.

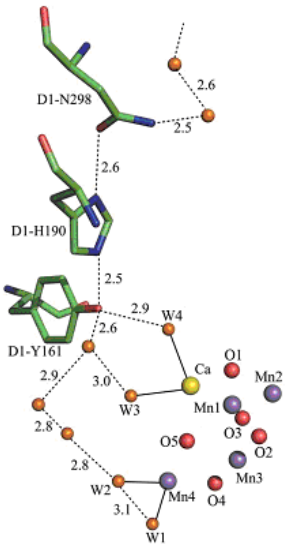

Figure3.14 *Hydrogen bonding network at oxygen evolving complex, two of them were bound to manganese, and another two waters bound calcium*. (Reprinted with permission from Nature Publishing Group).

In fact, this water hydrogen-bonding network at the OEC is necessary and important for water oxidation.[81b] Experiments show that disruption of this network destroys the steady state rate of S_1 to S_4 in water oxidation.

Hydrogen bonding networks are important in our calculated systems as well. In a realistic medium of water, the protic solvation effect is obvious and quite strong. In order to reproduce this effect accurately, we add two additional explicit water molecules to the aqua-Ru complex $(L)(pic)_2Ru^{III}$-OH_2 (L = hqc, pdc, H_2hqc = 8-hydroxyquinoline-2-carboxylic acid) in our calculations.[82] Two optimized geometries are shown in Figure 3.15:

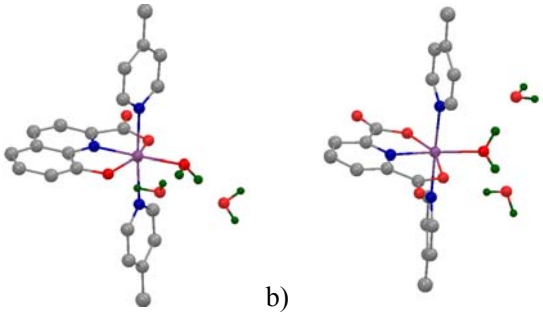

a) b)

Figure 3.15 *Calculated geometries of* $[Ru^{III}(hqc)(pic)_2{-}OH_2]^+$ *(a) and* $[Ru^{III}(pdc)(pic)_2{-}OH_2]^+$ *(b) in aqueous medium. Hydrogen atoms except those bonding to oxygen atoms are omitted for clarity. (Purple for Ru, grey for C, blue for N, red for O and green for H).*

One of the water molecules serves as both a hydrogen-bond donor and acceptor at the same time, the other one acts only as a hydrogen-bond acceptor. This hydrogen-bonding network could function as a channel for proton transfer and facilitate the Proton-Coupled Electron Transfer (PCET).

3.5 OO Bond Formation (O_2 Evolution)

The O-O bond formation is one of the most important steps in the oxygen evolution mechanism. After a stepwise and simultaneous loss of electrons and protons, the complexes are able to reach their higher oxidation states, which is required for the OO bond formation.

Generally, there are two main proposals for the key O-O bond formation event.[83-85] One is water, possibly a hydroxide ion, attack at the terminal oxo group (**WNA**). The other one is oxo-oxo coupling between two M=O units (**I2M**). The difference between these two pathways is whether a solvent water molecule is involved in the formation of OO bond or not. The two proposed OO bond formation pathways are shown in Table 3.2.

Table 3.2

WNA	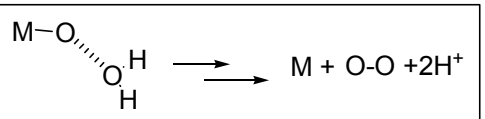
I2M	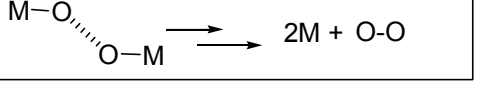

3.5.1 Water Nucleophilic Attack (WNA).

Water attack on the oxo group to give a terminal peroxide in the key OO bond forming step

When the transition metal complex reaches its higher oxidation state, it could undergo a water nucleophilic attack, forming a peroxidic intermediate, and finally release the oxygen while the empty position is coordinated by an incoming water.[86-89] The whole mechanistic proposal of WNA for water oxidation using Ru-based WOC is represented in Figure 3.16.

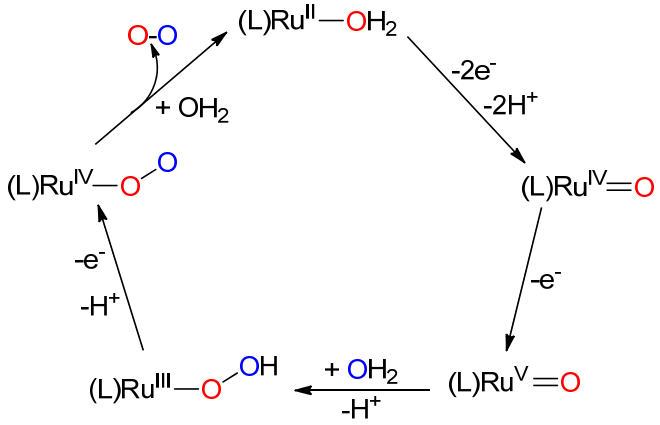

Figure 3.16 *Proposed OO bond formation mechanism based on the water nucleophilic attack.*

The complex Ru^{II}-OH_2 undergoes a sequential removal of electrons and protons to form Ru^{IV}-O, and it can reach an even higher oxidation state Ru^{V}-O. Once the Ru^{V}-O is formed, which is a highly reactive species, it undergoes a nucleophilic attack from a solvent water, then forms the terminal hydroperoxidic complex Ru^{III}-OOH, which contains the key feature of the O-O bond. The formed Ru^{III}-OOH intermediate can lose one more electron accompanied with one proton loss to form Ru^{IV}-OO, then releasing oxygen and finally coordinate a solvent water molecule. This **WNA** route was identified to be feasible for the well-known blue dimer (Figure 3.17).[90]

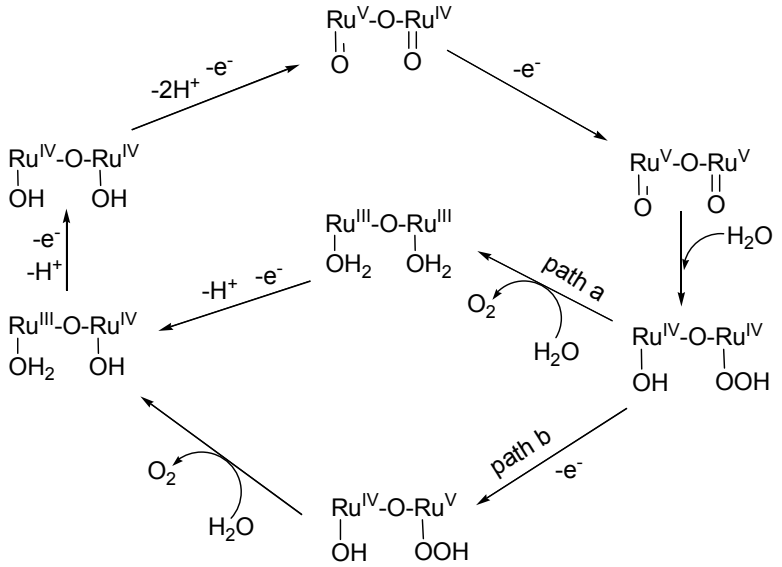

Figure 3.17 *Mechanistic proposal for O_2 generation using the blue dimer as catalyst. bpy ligands are omitted for clarity.*

The oxidation from H_2O-Ru^{III}-O-Ru^{III}-OH_2 to O-Ru^{V}-O-Ru^{V}-O was completed by a stepwise electron-proton removal. This product is a reactive and transient intermediate which is responsible for releasing oxygen when reacting with the solvent water. Once complex O-Ru^{V}-O-Ru^{V}-O was generated, it underwent a water nucleophilic attack immediately to form a HO-Ru^{IV}-O-Ru^{IV}-OOH intermediate. The following oxygen releasing step is dependent on the amount of Ce^{IV} oxidant.

If there is a stoichiometric amount of the Ce^{IV} oxidant, following path **a** HO-Ru^{IV}-O-Ru^{IV}-OOH intermediate generates oxygen and reforms the complex H_2O-Ru^{III}-O-Ru^{III}-OH_2, which is the initial form of blue dimer. However, the generation rate is relatively slow. If an excess of the Ce^{IV} oxidant is used, as path **b** shows, the HO-Ru^{IV}-O-Ru^{IV}-OOH intermediate will be further oxidized to O-Ru^{V}-O-Ru^{IV}-OOH, which releases oxygen much more rapidly, and then forms H_2O-Ru^{III}-O-Ru^{IV}-OH.

3.5.2 Interaction Between Two M-O Units (I2M).

Oxidative coupling of the two terminal oxo atoms of M=O.

The OO bond formation from the interaction between two M-O complexes includes two different manners, 1) Intramolecular approach, which means two M-O units are situated in one complex; 2) Intermolecular approach, which indicates that it is a bimolecular process, each complex contains only one M-O unit. Both pathways using Ru-based WOCs can be concluded in Figure 3.18.

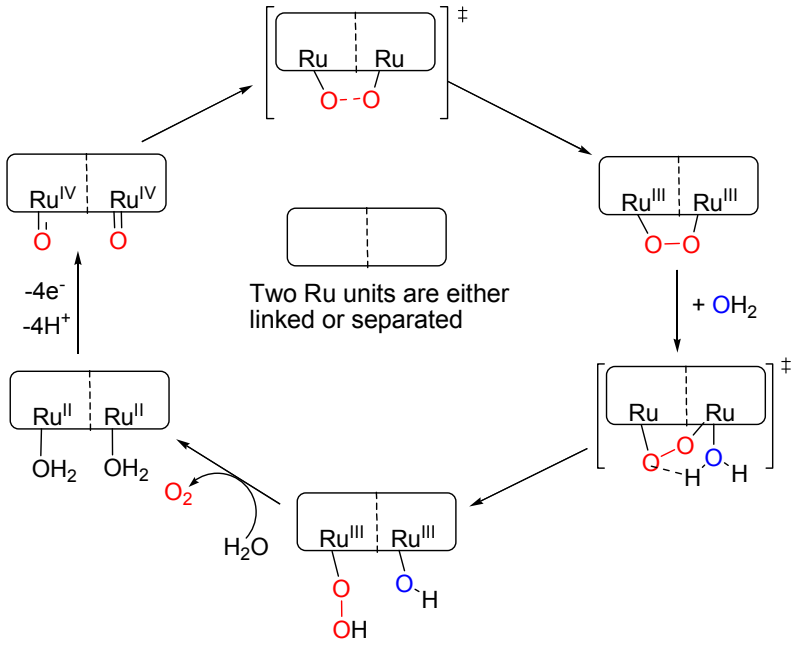

Figure 3.18 *General proposed OO bond formation mechanism based on interaction of two Ru-O units. (Both intramolecular and intermolecular pathways)*

3.5.2.1 Intramolecular Approach

For the complex in, in-$\{[Ru^{II}(trpy)(OH_2)]_2(bpp)\}^{3+}$ (in, in- Ru-Hbpp) (trpy is 2,2′:6′,2″-terpyridine, bpp is bis(2-pyridyl)-3,5-pyrazolate),[91] which contains two Ru-O units in the same complex, calculations show that the only OO bond formation mechanism occurring in this system is an intramolecular pathway (Figure 3.19), whereas the water nucleophilic attack mechanism is excluded.

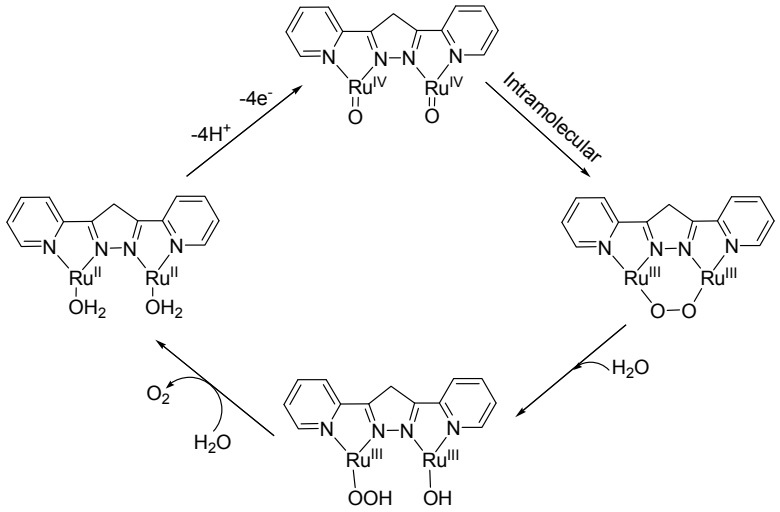

Figure 3.19 *Potential water oxidation mechanism for the in, in-Ru-Hbpp complex, and the trpy ligands are omitted for clarity.*

The complex H_2O-Ru^{II}-Hbpp-Ru^{II}-OH_2 is stepwise oxidized by Ce(IV) up to O-Ru^{IV}-Hbpp-Ru^{IV}-O. It then generates a Hbpp-1, 2-peroxo intermediate via an intramolecular interaction between two oxygen atoms, and this coupling reduces the Ru oxidation state from IV to III. A hydroperoxidic intermediate HOO-Ru^{III}-Hbpp-Ru^{III}-OH is then formed when one water molecule enters and it release oxygen finally with one more water coming in.

3.5.2.2 Intermolecular Approach.

OO bond formation via intermolecular coupling proposal was first reported by the Sun group, and the kinetics of catalytic water oxidation were tested to be second order in complex **3-6** Ru(bda)(pic)$_2$ (H_2bda = 2,2'-bipyridine-6,6'-dicarboxylic acid; pic = 4-picoline), which indicating that the catalytic reaction proceeds thought a dimeric complex.[92] Following this a computed binuclear pathway was completed by Privalov and coworkers in 2010.[93]

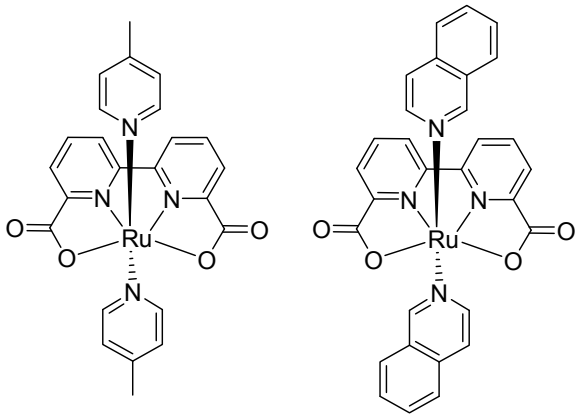

Figure 3.20 *Structures of complexes **3-6** and **3-7**.*

Another mono-ruthenium complex **3-7** Ru(bda)(isoq)$_2$ (isoq = isoquinoline) was also synthesized by Sun and coworkers (Figure 3.20). Especially complex **3-7** demonstrates superior catalytic performance on water oxidation using Ce^{IV} as the oxidant. It reaches an amazingly high reaction rate with a TOF of more than 400 s^{-1}. The performance of complex **3-7** is comparable to the oxygen-evolving complex in photosystem II, where the oxygen generation rate[94] in OEC is estimated at 100-400s^{-1}(light-driven).

The kinetic studies provided insight into the mechanism of OO bond formation. The kinetics of the catalytic reaction for water oxidation was identified as second order, which indicates the reaction proceeds in a bimolecular manner. A

radical coupling between two Ru-O units[95-98] was proposed to be involved in this key process.

Now we focus complex **3-6** for a detailed discussion. Normally the ideal angle for an octahedron configuration is 90º, however, for complex **3-6**, the O-Ru-O angle is expanded to 122.99º. It therefore can generate a seven-coordinated complex by accepting one incoming water molecule. After reaching its high oxidation state, it forms a seven-coordinate Ru^{IV} dimer μ–(HOHOH)-[Ru^{IV}(bda)(pic)$_2$]$_2$. The crystal structure of this dimer is shown in Figure 3.21.

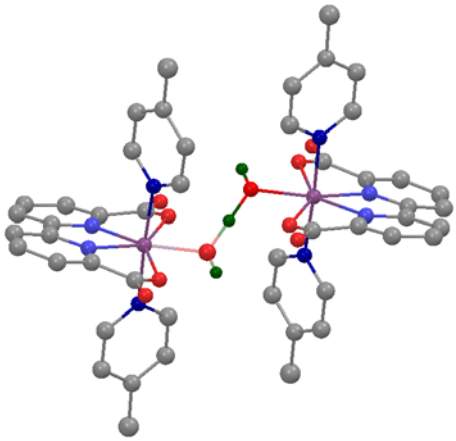

Figure 3.21 *Crystal structure of seven-coordinate Ru(IV) dimeric complex. Hydrogen atoms except those bonding to oxygen atoms are omitted for clarity. (Purple for Ru, grey for C, red for O, blue for N, and green for H).*

The calculated free energy barrier via a low-spin antiferromagnetic transition state is only 11.9 kcal/mol by taking the encounter complex as a reference. From the former computational study by Yang and Baik,[99] the dissociation of oxygen does not demand a high-energy ligand exchange from a peroxo intermediate. The general inter-molecular OO bond formation proposal is shown in Figure 3.22.

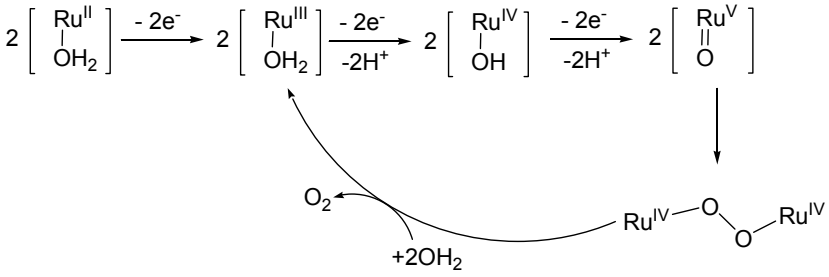

Figure 3.22 *General description of oxygen evolution with inter-molecular coupling pathway.*

Both electronic and geometrical properties of the bda ligand make a

contribution on the formation of a seven-coordinate complex, which is essential for generation of seven-coordinate dimer afterwards. OO bond formation was proposed from the bi-nuclear coupling for the first time.

Chapter 4

Natural Hydrogenases and Synthetic Mimic Complexes

4.1 Brief Introduction

Hydrogen (H_2) has the potential to be the clean energy carrier of the future by replacing fossil fuels, particularly if we can produce it by water splitting using visible light. As an energy carrier and potential transportation fuel, hydrogen (H_2), a closed-shell molecule has been envisioned.[100,101] Hydrogen is an ideal fuel, which can be generated from water, and the only product of the reaction is water when combustion of hydrogen is made with pure oxygen. It can therefore conform to the requirement of sustainability, energy security and environmental-benign character. Furthermore, hydrogen is one of the fuels which has highest specific energy, and the energy density of hydrogen can reach 33.3 kWh/kg (30 MPa),[102] this indicates it can release 33.3 kWh/kg of energy for every one kilogram. This number is much higher than that of gasoline (12.7 kWh/kg) which is frequently used in our daily life. Finding new ways to store hydrogen is therefore one of the main targets we are facing now.

Hydrogen is also involved in several key chemical processes, such as hydrogenation of inorganic and organic compounds which affects our daily life greatly. For example, ammonia fertilizer is necessary for human society to survive and develop since we need to feed the growing population by increasing the production of agricultural products.[103,104] In addition, further efforts are needed to remove sulfur and nitrogen from hundreds of million tons of crude oil to keep a

high quality,[105] and hydrogen is used for this purpose.

Although hydrogen is playing and continues to play an important role in our daily life, the economical production or the uptake of molecular hydrogen is limited by the intrinsic kinetic properties. Usually hydrogen is not reactive at ambient temperature. It can react with oxygen to form water, however, this reaction is slow at room temperature. The hydrogen was even treated as an "inert" gas in air-free chemistry a long time ago because of its stable chemical properties although it is now replaced by N_2 or Argon.

The following physical and chemical properties [106] could provide part of the explanation for the unreactive property of hydrogen:

(1) Hydrogen is a completely nonpolar molecule;

(2) The bond between H-H is remarkably strong, and the required energy for homolytic cleavage of an H-H bond is 103 kcal/mol;

(3) Due to the high basicity of hydride (H^-) molecular hydrogen is a poor acid.

Since the H-H bond is generally stronger than most new H-X bonds, chemists place the H-H bond into the strongest single bond category. The design of effective catalysts for hydrogen oxidation and proton reduction becomes a challenge. Because of the intrinsic thermodynamic limitations, molecular hydrogen production/uptake is currently only economically viable under high temperature conditions or in presence of a platinum catalyst.[107,108]

4.2 Hydrogenase Enzymes

The natural hydrogenases[109-113] serve as good models for hydrogen uptake/production. Hydrogenases are billion-year old redox enzymes and frequently present in microorganisms belonging to the Archaea and Bacteria domains of life, a few of them are found in Eukarya as well.[114] They display a remarkable performance on the reversible inter-conversion between protons and hydrogen, since the purpose of hydrogenase enzymes is to set a charge separation or combination. Consequently, synthetic catalysts with simpler structure based on these hydrogenase enzymes have been studied.

Most of the hydrogenase enzymes[115] can be divided into two major classes by specifying the transition metal they carry: Ni-Fe and Fe-only hydrogenases. Ni-Fe hydrogenases are primarily used for hydrogen uptake, whereas the Fe-Fe hydrogenases are usually used for proton reduction.

4.2.1 Ni-Fe Hydrogenases

The Ni-Fe hydrogenases[116,117] are mainly used for the heterolytic cleavage of hydrogen. The X-ray crystal structure of the oxidized form of Desulfovibrio gigas of a Ni-Fe hydrogenase was obtained at a resolution of 2.85 Å for the first time in 1995,[118] and from then on X-ray crystal structures from other organisms have been obtained.[119-121]

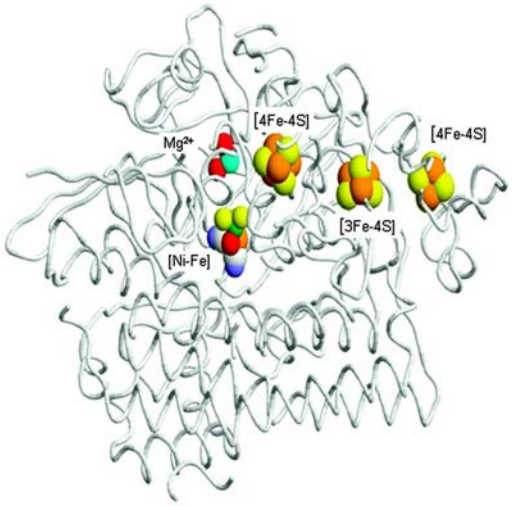

Figure 4.1 *The crystal structure of nickel-iron hydrogenases purified from D. gigas. (Reprinted with permission from ACS publications)*

As shown in Figure 4.1, a nickel atom is situated in the active site, a chain of three iron-sulfur clusters consists of one [3Fe-4S] cluster and two cubane type clusters contain eleven iron atoms.[122]

4.2.2 Fe-Fe Hydrogenase

Iron-iron hydrogenases[123-126] are generally found capable of reducing protons, although some of them are used for hydrogen oxidation and occasionally bi-directionality have been observed. For molecular structures of Fe-Fe hydrogenases, there are many different sources, scientists still found many structural similarities among them although the structures of them are even slightly different from each other under different crystallization states. The main structures were concluded from the X-ray crystallographic information of Desulfovibrio desulfuricans Hildenborough (*DdH*) and Clostridium pasteurianum I (*CpI*)[127-129] (Figure 4.2), which are hydrogen uptake and hydrogen production enzymes, respectively.

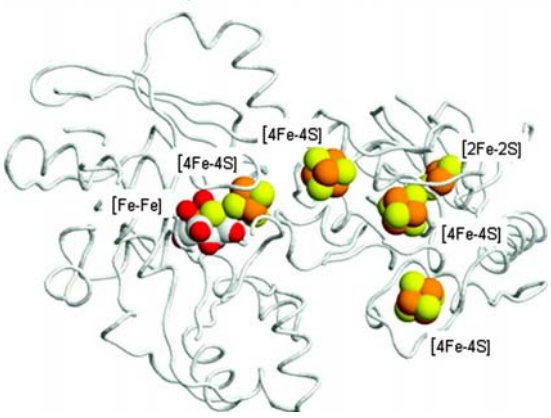

Figure 4.2 *The crystal structure of Clostridium pasteurianum I (CpI) iron-iron hydrogenase. (Reprinted with permission from ACS publications)*

The consensus structure[130] of the active site of Fe-Fe hydrogenase is shown in Figure 4.3,

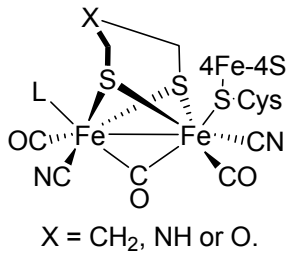

Figure 4.3 *The consensus structure of the active site of Fe-Fe Hydrogenase.*

Furthermore, the Fe-Fe hydrogenases are well known for their abilities to reduce protons to hydrogen, at nearly Nernstian potentials the turnover frequencies of Fe-Fe hydrogenase enzymes can reach a value of around 6000 mol of H_2/mol per hydrogenase enzyme per second. Many scientists are inspired by the amazing catalytic performance of proton reduction/hydrogen uptake with hydrogenases. Therefore, many variations of electrochemical and photochemical hydrogen production/uptake systems based on Fe-complexes have been created. Numerous studies both experimentally and theoretically focus on these artificial systems.

4.3 Homogeneous Light-Driven Catalytic Systems

After studying the structures of hydrogenase enzymes, we found that the first-row transition metals, such as iron and nickel, are usually present in catalysts for a catalytic hydrogen uptake/production. This discovery results in a fast development of hydrogenase modelization, therefore many studies have been devoted to synthesize much smaller molecular complexes to mimic the structure and function

of these hydrogenase enzymes.

In addition, hydrogen generation using renewable energy such as solar energy could be an ideal method for sustainable production and storage of energy, and many scientific groups has focused their attention on water splitting during last 30 years.[131-138] It is important to emphasize that most of work in this field was devoted to heterogeneous photocatalytic systems,[139-141] while homogeneous ones were poorly developed. However, during the past few years much progress has been achieved in developing and understanding homogeneous photocatalytic systems.[142-146]

Recently, Mei Wang and coworkers designed a system[147] (Figure 4.4) comprising of 1) Photosensitizer, usually based on the ruthenium tris-bpy moiety; 2) A catalytic center based on a transition metal complex; 3) A redox mediator.

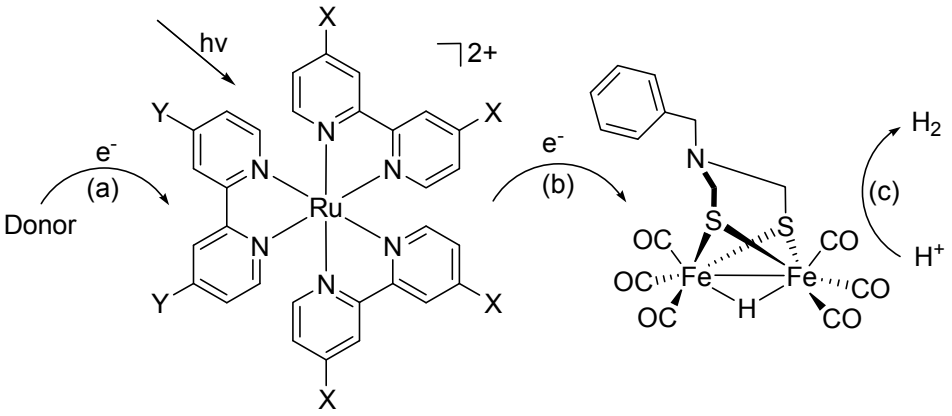

(a) reductive quenching; (b) intermolecular ET; (c) catalytic proton reduction

Figure 4.4 *Homogeneous light-driven catalytic systems based on Fe for hydrogen production using ruthenium-polypyridine as photosensitizer.*

However, homogeneous light-driven catalytic systems for hydrogen production remain relatively rare in experimental phase. A practical technology for hydrogen generation derived from solar energy remains a goal to be achieved.

4.4 Effect of the Pendant Base in Iron-Complexes.

The transport or movement of proton[148-151] is vital in many biological and chemical processes including the hydrogen oxidation/production, the reduction of CO_2 to formate and the reduction of O_2 to water. It is often related to energy storage and utilization, however the details of these processes are still ambiguous. Internal amine base is a reoccurring feature of hydrogenases. It is likely to facilitate the proton transfer to the metal center. For natural hydrogenase enzymes or synthetic catalysts based on iron or nickel, we found that the incorporation of a

pendant amine is a frequently occurring feature, the pendant amine base is located in proximity of the metal and forms a weak interaction with the metal since it is too far away to form a strong bond.[152] Many research groups have also reported aza and oxadithiolates as probable proton relays[153-158] in functional models for the Fe-Fe hydrogenases, and are dedicating their efforts to this process, aiming at providing understanding for their functions.

4.4.1 Pendant Base Effect on Proton Transfer in Iron-Complex

Three complexes **4-1** $Fe_2(pdt)(CO)_2(dppv)_2$, **4-2** $Fe_2(adt)(CO)_2(dppv)_2$ and **4-3** $Fe_2(odt)(CO)_2(dppv)_2$ (dppv = cis-1,2-bis(diphenylphosphino)ethylene; pdt = 1,3-propanedithiolate; adt = 2-azapropane-1,3-dithiolate; odt = 2-oxopropane-1,3-dithiolate) were synthesized, and all these complexes are with a dithiolate moiety which acts as a bridge between the two iron subunits.[159] Rauchfuss and coworkers proposed that the functionality of amine in complex **4-2** could act as a proton relay that transfers the proton from and to the bridging site between the two Fe atoms.

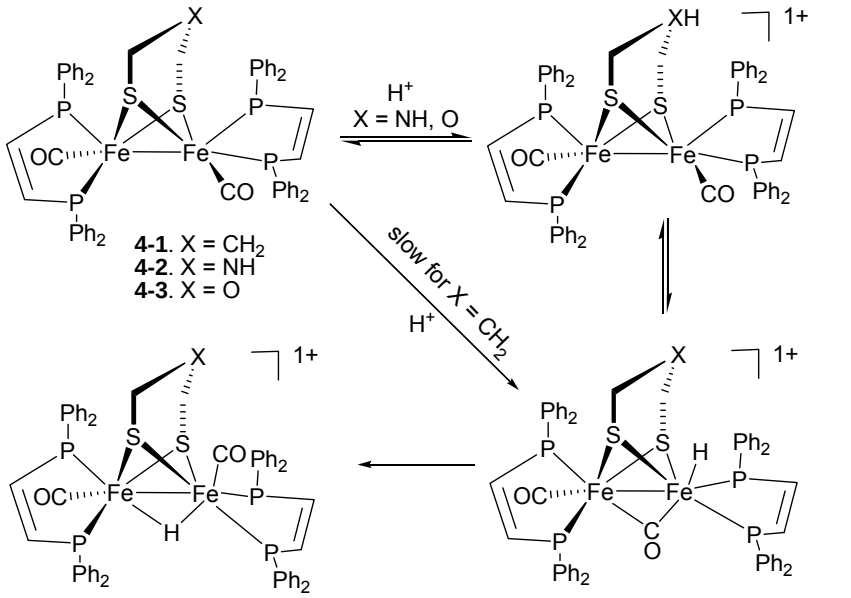

Scheme 4.1 *Proton relay effect of heteroatom in the dithiolate.*

Scheme 4.1 demonstrates how a heteroatom in the dithiolate shuffles proton to and from the metal iron. All these complexes **4-1**, **4-2** and **4-3** were found to be protonated with a strong acid $[H(Et_2O)_2]BAr^F{}_4$ quickly at -90℃, however, only complex **4-2** can be protonated if a billion-fold weaker acid $[HPMe_2Ph]BF_4$ was used instead, even though these diiron complexes have similar basicities. This

difference indicates that the presence of a heteroatom N exerts a strong effect on the rate of protonation. Their results suggested that in complex **4-2** the protonation initially happens at the amine base, then transfers to the terminal site, and finally reaches the bridging site. In contrast, for complex **4-1** that contains nonbasic propanedithiolate or complex **4-3** with a weakly basic oxadithiolate, the initial protonation on the internal base is blocked.

They also compared the deprotonation of all terminal hydride complexes [**4-1**(*t*-H)]$^+$, [**4-2**(*t*-H)]$^+$, [**4-3**(*t*-H)]$^+$. For complex [**4-1**(*t*-H)]$^+$, even at room temperature it is impossible deprotonate using any organic base, and it isomerizes to bridging complex eventually. For complex [**4-3**(*t*-H)]$^+$, it is inert toward base at -78℃, however it will generate two products **4-3** and [**4-3**(μ-H)]$^+$ slowly when the temperature increase to around 0℃. Neither the concentration nor the pK_a of the base has any influence on the proportion of these two products. It is quite different in the case of [**4-2**(*t*-H)]$^+$, the deprotonation of it occurs immediately with a base of PBu_3[$HPBu_3$] BF_4 even at a rather low temperature of -90℃, and the only observed product is complex **4-2**.

Since there is almost no difference in the υ_{CO} region among these three complexes in the IR spectra, the thermodynamic acidities of them should be the similar. This demonstrates that the big difference of the deprotonation rate among them lies in the presence of the heteroatom.

In summary, complex **4-2** shows that the heteroatom N facilitates the protonation and relay the proton to Fe immediately, and complex **4-3** which contains a relatively weakly basic oxadithiolate shows a moderate performance although inferior of complex **4-2**. Complex **4-1** with a non-basic propanedithiolate is inert to both protonation and deprotonation.

4.4.2 Pendant Amine Base Effect on Heterolytic Activation of Hydrogen in Iron-Complex

The pendant amine base is not only involved in the intramolecular proton transfer but also related to the heterolytic activation of hydrogen. Computational and experimental studies were used to provide insight into the details of heterolytic splitting of hydrogen, which takes place at the incorporated pendant amine and the metal core (Scheme 4.2).

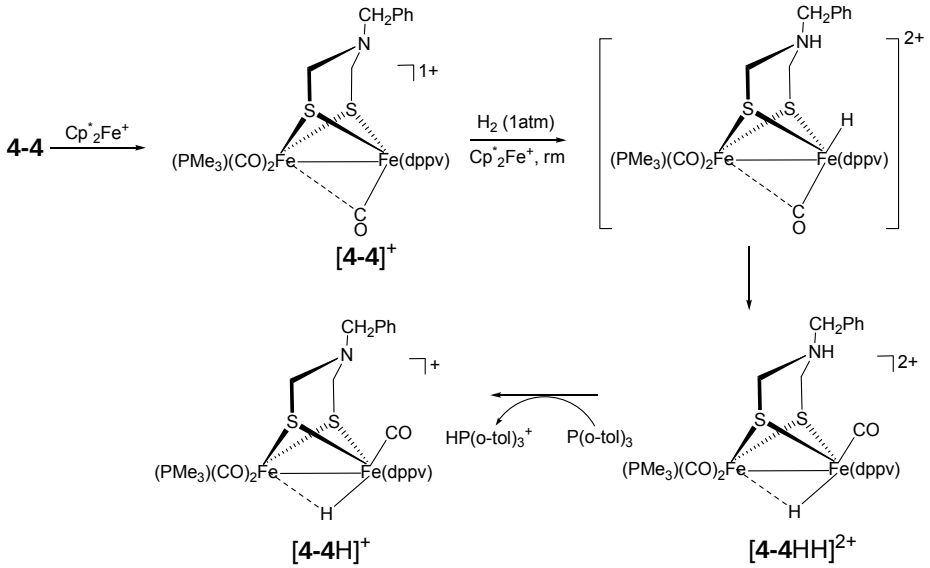

Scheme 4.2 *The pendant amine base facilitates the heterolytic activation of hydrogen.*

Complex **4-4**[160] $Fe_2[(SCH_2)_2NBn](CO)_3$-(dppv)(PMe_3) first loses one electron to generate [**4-4**]$^+$ to the mild oxidant $[Fe(C_5Me_5)_2]^+$, then [**4-4**]$^+$ participates in the heterolytic activation of hydrogen, one situated at the pendant amine base N position, while another one is located at the Fe atom. This internal base makes a contribution to the stabilization of the heterolytically cleaved species. The cleavage first generates a terminal hydride intermediate, which isomerizes to a more stable form the bridging hydride complex [**4-4**HH]$^{2+}$. The proton at the N site is trapped by P(o-tol)$_3$, and yields [**4-4**H]$^+$ as the final product.

The two cases we described above indicate that the pendant amine bases are important in proton transfer or movement. In fact, this proton transfer or movement in the complex is a vital part of the mechanistic study of hydrogen generation and uptake, and pendant amine base plays an important role in this kind of proton movement or transfer. However, the need for this proton relay function has not been clearly explained. It is therefore necessary for us to study and provide further explanation on the role the pendant base. We believe that a thorough understanding of proton relays will be crucial for developing efficient hydrogen production and hydrogen oxidation catalysts.

4.5 Hydrogen activation/generation by Iron-Complexes.

Structural and functional mimicking of the active site of hydrogenase is gathering more and more attention recently. Proton reduction is closely related to energy

storage from water splitting by production of H_2; and H_2 oxidation is related to energy release in a fuel cells by H-H bond cleavage.

4.5.1 Hydrogen Oxidation in Iron-Complexes

One H_{ox} state complex [**4-5**]$^+$ [(μ-pdt){Fe(CO)$_3$}{Fe(μ-CO)(κ^2-Ph$_2$PCH$_2$N(*n*-Pr)CH$_2$PPh$_2$)}] (pdt = propane-1,3-dithiolate) for H_2 oxidation was reported by Sun's group recently.[161] The structure of [**4-5**]$^+$ with a vacant apical site and a semi-bridging CO was determined by X-ray crystallography. It exhibits catalytic activity for H_2 oxidation in the presence of excess oxidant and base under mild conditions (1 atm, 25 ℃) (Figure 4.3).

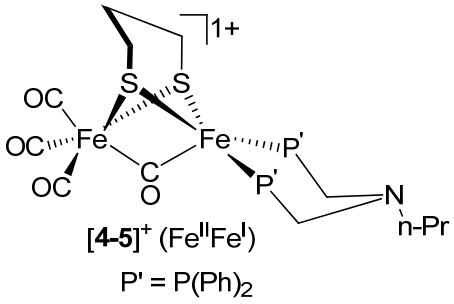

Figure 4.3. *Molecular structure of complex **4-5**.*

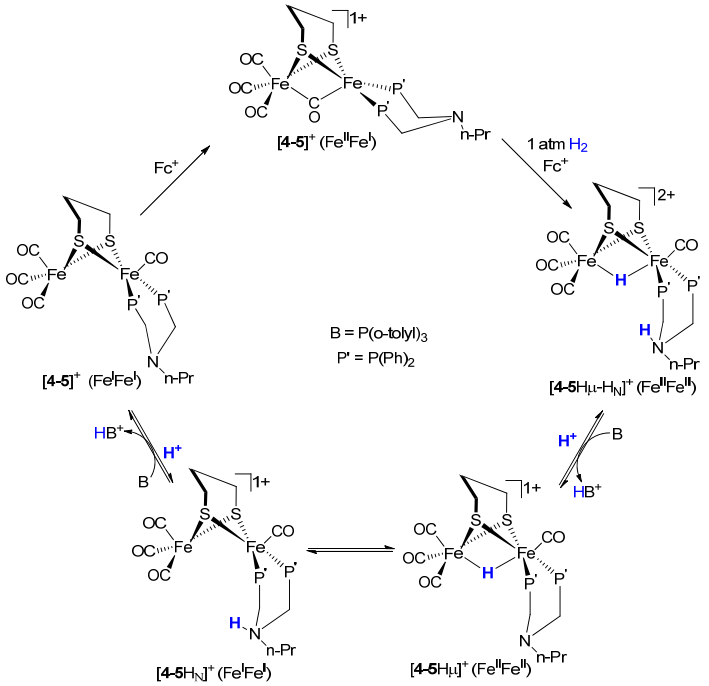

Scheme 4.1. *A possible pathway for catalytic H_2 activation by complex **4-5**.*

A proposed pathway for catalytic H_2 activation by complex [**4-5**]$^+$ in the

presence of excess Fc^+ and $P(o\text{-}tol)_3$ is shown in Scheme 4.1.

4.5.2 Hydrogen Generation in Iron-Complexes

One biomimetic catalyst for hydrogen generation with the amine cofactor (adt^{NH}) **4-6**^{NH}, $Fe_2(adt^{NH})(CO)_2(dppv)_2$, [$(adt^{NH})^{2-}$ = $HN(CH_2S)_2^{2-}$, pdt^{2-} = 1,3-$(CH_2)_3S_2^{2-}$, and dppv = cis-$C_2H_2(PPh_2)_2$] has been reported by the Rauchfuss group.[162]

Protonation of **4-6**^{NH} under weakly and strongly acidic conditions gives the terminal hydride [*t*-H**4-6**^{NH}]$^+$ and ammonium hydride [*t*-H**4-6**^{NH2}]$^{2+}$, respectively (Figure 4.4). The species [*t*-H**4-6**^{NH2}]$(BF_4)_2$ represents the first example of terminal hydride produced by protonation determined by X-ray crystallography.

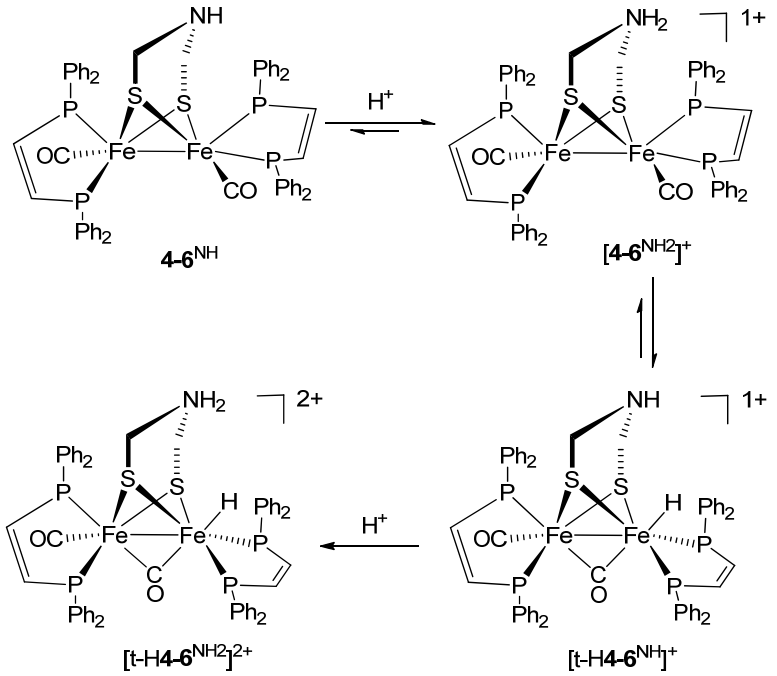

Figure 4.4. *Protonation of **4-6**^{NH} under weak and strong acids gives the terminal hydride [t-H**4-6**^{NH}]$^+$ and ammonium hydride [t-H**4-6**^{NH2}]$^{2+}$, respectively.*

The catalytic activity of [*t*-H**4-6**^{NH}]$^+$ is closely related to the property of acids, it proceeds at TOF of 5000 s^{-1} with an over-potential of 0.7 V when using a relatively weak acid. The ammonium hydride [*t*-H**4-6**^{NH2}]$^{2+}$ proceeds much faster, with an estimated TOF of 58000 s^{-1} and an over-potential of 0.5 V. The proposed mechanism for H_2 evolution (two sub-cycles for strong and weak acids, respectively) by [*t*-H**4-6**^{NH}]$^+$ is shown in Scheme 4.2.

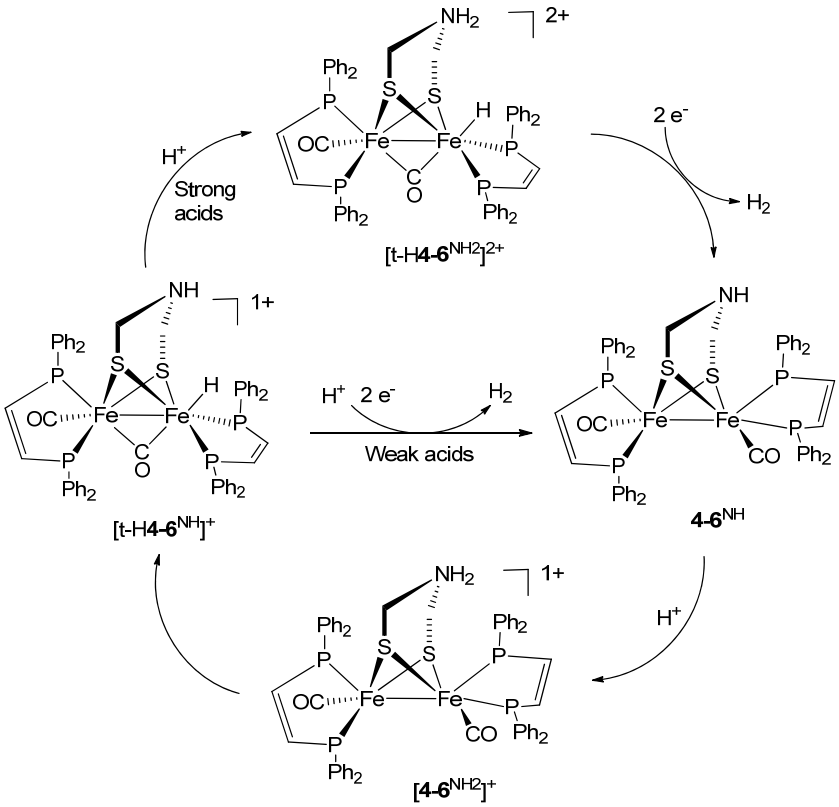

Scheme 4.2. *Proposed mechanism for H_2 evolution by [t-H**4-6**^{NH}]$^+$. Two sub-cycles are shown for strong and weak acids.*

Chapter 5

Summary of Included Papers

A brief summary of papers included in this thesis and our contributions to them are presented in this chapter.

5.1 Theoretical Studies on Water Oxidation Using Ru-based Catalysts.

Paper I. One combined (experimental and theoretical) study of complexes **1**–**3**, including $Ru^{II}(hqc)(pic)_3$ (**1**), $Ru^{II}(pdc)(pic)_3$ (**2**) and $Ru^{II}(tpy)(pic)_3$ (**3**) (H_2hqc = 8-hydroxyquinoline-2-carboxylic acid; H_2pdc = 2,6-pyridine-dicarboxylic acid; tpy = 2,2':6',2''-terpyridine; pic = 4-picoline) was presented in this paper. Our results revealed the effect of anionic ligands on the catalytic water oxidation, and the negatively charged ligands, including hqc and pdc, clearly increase the rate of ligand substitution between picoline and water. This ligand exchange was proposed to proceed through a dissociative mechanism. Furthermore, the anionic oxygen donors, such as phenolate and carboxylate, can labilize the Ru^{III}–N(pic) bond. These findings could be the explanation why Ru complexes bearing anionic ligands exhibit much better performance.

Paper **II**. The interest in the reactivity of ruthenium complexes with water is related to light-driven water splitting, which has attracted much attention in recent years due to its potential to convert solar energy to chemical energy. The results in this paper add a new angle to the understanding of water oxidation catalysts. An extensive study of the reaction between water and a Ru(V)=O species was presented in this paper. The product of this reaction has never been characterized

or isolated so far, and has been proposed to be a Ru(III)-OOH species in most cases. In this paper we found that reaction of water at the Ru center instead of the oxo site had a much lower activation free energy. The intermediate formed is a seven-coordinate species, which can rearrange into a slightly more stable six-coordinate Ru species with hydroxide coordinated instead of one of the original ligands. The consequence of this finding is that that the observed disappearance of the Ru(V)=O may need to be reinterpreted. It opens up for completely new catalytic pathways, possibly involving even higher oxidation states or reactions of the seven coordinate intermediates.

Paper **III**. With this paper we finally completed the entire mechanistic research on water oxidation, and an extensive study of OO bond formation and O_2 release with **1** $[(bpc)(bpy)Ru^{II}OH_2]^{1+}$ (Hbpc = 2,2'-bipyridine-6-carboxylic acid, bpy = 2,2'-bipyridine) is presented in this paper. Stepwise oxidation via proton-coupled electron transfer gives **3** $[(bpc)(bpy)Ru^{IV}=O]^{1+}$. An active **4** $[(bpc)(bpy)Ru^{V}=O]^{2+}$ which is involved in the OO bond formation is generated with a further $1e^-$ oxidation of **3**. The OO bond formation via a water nucleophilic attack at **4** is considered as the rate-determining step in this water oxidation catalytic cycle, and the hydro-peroxo **6** $[(bpc)(bpy)Ru^{III}OOH]^{1+}$ is generated accompanied with one proton transfer. The super-oxo $\mathbf{7}_{\mathbf{side\text{-}on}}$ $[(bpc)(bpy)Ru^{IV}OO]^{1+}$ and $\mathbf{8}_{\mathbf{side\text{-}on}}$ $[(bpc)(bpy)Ru^{V}OO]^{2+}$ (both are in low spin state) are generated by further oxidations of **6**. Our calculation results demonstrate that oxygen release can happen at both Ru^{IV} and Ru^{V} states. $\mathbf{7}_{\mathbf{side\text{-}on}}$ and $\mathbf{8}_{\mathbf{side\text{-}on}}$ need to transform to their high spin states (end-on configurations) by a spin crossing, $\mathbf{10}_{\mathbf{end\text{-}on}}$ and $\mathbf{14}_{\mathbf{end\text{-}on}}$ respectively, before releasing O_2. Following a dissociated pathway O_2 is generated, and oxygen release is found to be plausible in both pathways. From the overall free energy surface of this catalytic cycle, the OO bond formation is considered to be the rate-determining step in this water oxidation catalytic cycle with the catalyst **1**.

5.2 Theoretical Studies on Proton Transfer and Proton Reduction Using Fe-based Catalysts.

Paper **IV**. Most natural hydrogenases and biomimetic catalysts use pendant amine bases to assist their functions. By using density functional theory on [FeFe]-hydrogenase mimics we found that pendant amine bases speed up the proton transfer to and from metal centers by dividing the high free energy barrier

into one mainly entropic barrier and one mainly enthalpic. We find that the enthalpic barrier for deprotonating the metal center is relatively high. This prohibits deprotonation by an external base since associating the base with the metal complex will lead to a decrease in entropy and thus a higher free energy barrier. The pendant amine has a similar enthalpic barrier to the external base, however, since it is covalently linked to the metal complex, and the loss of entropy is minimal and the free energy barrier within reach. Once the proton is at the amine base it can be transferred to the external base in a reaction with a barrier that is dominated by the entropic contribution for associating two molecules, and with a minimal enthalpic barrier.

Paper **V**. This investigation examines four different possible pathways for deprotonation of [(μ-pdt){Fe(CO)$_3$}{Fe(CO)(κ^2-Me$_2$PCH$_2$N(Me)CH$_2$PMe$_2$)}] (pdt = propane-1,3-dithiolate) [**1**H$_\mu$]$^{1+}$, including 1) the "Direct" deprotonation; 2) the "Indirect" deprotonation via the pendant amine N; 3) the "Indirect" deprotonation via the distal metal Fe; 4) the "Indirect" deprotonation via the dithiolate group S. We found out that only the first one, which is "Indirect" pathway via the pendant amine N results in a reasonable free energy barrier, which can be overcome smoothly at room temperature. The pendant amine N is the most favourable migration destination for the bridging hydride in [**1**H$_\mu$]$^{1+}$, while migrations to other possible positions such as distal metal Fe or S of the dithiolate require much higher activation energy. However, once the migration barriers of three "Indirect" pathways are overcome, deprotonations from all three sites including the core atom Fe, S and N, are all available. Our results also indicate one significant difference for deprotonation of the hydride from the terminal and bridging sites. The low energy of the virtual orbital associated with the antibonding M-H interaction of [**1**H$_{Fe}$]$^{1+}$ explains the high activity for the interaction with aniline. The pendant amine N can play a positive role in preventing the formation of bridging hydride complex, which is usually the most stable form of protonated iron complex.

Paper **VI**. One mechanistic study on modeling of the H$_{ox}$ state for H$_2$ activation was also completed in this thesis by using DFT. Our results implied that the most favorable reaction path involves a rotation of the bridging CO to an apical position firstly, then followed by H$_2$ activation to give a bridging hydride intermediate with the assistance of the internal base. Our results can shed light on the molecular details of hydrogen generation, and serve as a guideline in the development of new catalysts.

References

[1] Lewis, N. S.; Nocera, D. G. *Proc. Nat. Acad. Sci. USA*., **2006**, 103, 15729-15735.

[2] Lewis, N. S. In *Energy and Transportation*; *The National Academies Press: Washington, DC*, **2003**, p33.

[3] Braber, J.; Andersson, B. *Nature*, **1994**, 370, 31-34.

[4] Renger, G. *Physiol. Plant.*, **1997**, 100, 828-841.

[5] Pecoraro, V. L.; Hsieh, W. Y. *Inorg. Chem*., **2008**, 47, 1765-1778.

[6] Barber, J. *Inorg. Chem*., **2008**, 47, 1700-1710.

[7] a) Yano, J.; Yachandra, V. K. *Inorg. Chem*., **2008**, 47, 1711-1726; b) Ananyev, G. M.; Dismukes, G. C., *Photosynth. Res*, **2005**, 84, 355-365.

[8] Gust, D.; Moore, T. A.; Moore, A. L. *Acc. Chem. Res*., **2009**, 42, 1890-1898.

[9] a) Yagi, M.; Syouji, A.; Yamada, S.; Komi, M.; Yamazaki, H.; Tajima, S.*Photochem. Photobiol. Sci.*, **2009**, 8, 139-147; b) Lomoth, R.; Magnuson, A.; Sjodin, M.; Huang, P.; Styring, S.; Hammarström, L. *Photosynth. Res.,* **2006**, 87, 25-40; c) Sun, L-C.; Hammarström, L.; Åkermark, B.; Styring, S. *Chem. Soc. Rev*., **2001**, 30, 36-49.

[10] Dempsey, J. L.; Esswein, A. J.; Manke, D. R.; Rosenthal, J.; Soper, J. D.; Nocera, D. G., *Inorg. Chem*., **2005**, 44, 6879-6892.

[11] a) Grätzel, M. *Nature*, **2001**, 414, 338-344. b) Domen, K.; Naito, S.; Soma, M.; Onishi, T.; Tamaru, K. *Chem. Commun*, **1980**, 543-544. c) Reece, S. Y.; Hamel, J. A.; Sung, K.; Jarvi, T. D.; Esswein, A. J.; Pijpers, J. J. H.; Nocera, D. G.; *Science*, **2011**, 334, 645-648.

[12] Jensen, F. *Introduction to Computational Chemistry*. Second Edition, **2007**.

[13] Szabo, A.; Ostlund, N. S. *Modern quantum chemistry: introduction to advanced electronic structure theory*, Courier Dover Publication, **1996**.

[14] Levine, I. N. *Quantum chemistry*. Pearson Prentice Hall, **2009**.

[15] Helgaker, T.; Jorgensen, P.; Olsen, J. *Molecular electronic-structure theory*, Wiley, **2000**.

[16] McWeeny, R.; Sutcliffe, B. T. *Methods of molecular quantum mechanics*; Academic Press, **1969**.

[17] Pilar, F. L. *Elementary quantum chemistry*; Courier Dover Publications, **2001**.

[18] Møller, C.; Plesset, M. S. *Phys. Rev*., **1934**, 46, 618-622.

[19] Thomas, L. H. *Proc. Cambridge Phil. Soc*., **1927**, 23, 542-548.

[20] Fermi, E. *Rend. Accad. Naz. Lincei.*, **1927**, 6, 602-607.

[21] Dirac, P. A. M. *Proc. Cambridge Phil. Soc*., **1930**, 26, 376-385.

[22] Hohenberg, P.; Kohn, W. *Phys. Rev*., **1964**, 136, B864-B871.

[23] Burke, K. *J. Chem. Phys*., **2012**, 136, 150901-150901.

[24] Kohn, W. Sham, L. J. *Phys. Rev*., **1965**, 140, A1133-A1138.

[25] Perdew, J. P. *Phys. Rev. B.,* **1986**, 33, 8822.

[26] Becke, A. D. *J. Chem. Phys*., **1993**, 98, 5648-5652.

[27] Lee, C.; Yang, W.; Parr, R. G. *Phys. Rev. B.,* **1988**, 37, 785-789.

[28] Bauschlicher Jr, C. W. *Chem. Phys. Lett.*, **1995**, 246, 40-44.

[29] Curtiss, L. A.; Redfern, P. C.; Raghavachari, K. *J. Chem. Phys*., **2005**, 123, 124107-124111.

[30] a) Zhao, Y.; Truhlar, D. G. *Theor. Chem. Acc.,* **2008**, 120, 215-241; b) Zhao, Y.; Truhlar, D. G. *J. Phys. Chem. A*., **2006**, 110, 13126-13130.

[31] Zhao, Y.; Truhlar, D. G. *J. Phys. Chem. C*., **2008**, 112, 6860-6868.

[32] Grimme, S. *J. Chem.Phys.*, **2006**, 124, 34108-34116.

[33] Schwabe, T.; Grimme, S. *Phys. Chem. Chem. Phys*., **2007**, 9, 3397-3406.

[34] a) Li, J.; Fisher, C. L.; Che, J.; Bashford, D.; Noodleman, L. *Inorg. Chem*. **1996**, 35, 4694-4702; b) Tavernelli, I.; Vuilleumier, R.; Sprik, M. *Phys. Rev. Lett*. **2002**, 88, 213002-213004.

[35] a) Eyring, H. *J. Chem. Phys*., **1935**, 3, 107-115; b) Laldler, K. J.; Klng, M. C. *J. Phys. Chem*., **1983**, 87, 2657-2664.

[36] a) Hwang, S.; Jang, Y. H.; Chung, D. S. *Bull. Korean. Chem. Soc.*, **2005**, 26, 585-588; b) Jang, Y. H.; Goddard III, W. A.; Noyes, K. T.; Sowers, L. C.; Hwang, S.; Chung, D. S. *Chem. Res. Toxicol*., **2002**, 15, 1023.

[37] Marten, B.; Kim, K.; Cortis, C.; Friesner, R. A.; Murphy, R. B.; Ringnalda, M.

N.; Sitkoff, D.; Honig, B. *J. Phys. Chem. A*., **1996**, 100, 11775-11788.

[38] Martin, J.M.L.; Sundermann, A. *J. Chem.Phys.,* **2001**, 114, 3408-3420.

[39] Tissandier, M.D.; Cowen, K.A.; Feng, W.Y.; Gundlach, E.; Cohen, M.H.; Earhart, A.D.; Coe, J.V. *J. Chem. Phys. A.,* **1998**, 102, 7787-7794.

[40] a) *BASIC RESEARCH NEEDS FOR SOLAR ENERGY UTILIZATION*, Report on the Basic Energy Sciences Workshop on Solar Energy Utilization, **2005**; b) Hadjipaschalis, I.; Poullikkas, A.; Efthimiou, V. *Renew Sust Energ Rev.*, **2009**, 13, 1513-1522.

[41] Liu, X.; Wang, F. *Coord. Chem. Res*., **2012**, 256, 1115-1136.

[42] Siegbahn, P. E. M. *Inorg. Chem*., **2008**, 47, 1779-1786.

[43] Barber, J. *Inorg. Chem*., **2008**, 47, 1700-1710.

[44] Yano, J.; Yachandra, V. K. *Inorg. Chem*., **2008**, 47, 1711-1726.

[45] Pecoraro, V. L.; Hsieh, W. Y. *Inorg. Chem*., **2008**, 47, 1765-1778.

[46] Limberg, J.; Szalai, V. A.; Brudvig, G. W. *J. Chem. Soc, Dalton, Trans.*, **1999**, 1353-1361.

[47] Blakemore, J. D.; Schley, N. D.; Balcells, D.; Hull, J. F.; Olack, G. W.; Incarvito, C. D.; Eisenstein, O.; Brudvig, G. W.; Crabtree, R. H. *J. Am. Chem. Soc*., **2010,** 132, 16017-16029.

[48] Sens, C.; Romero, I.; Rodriguez, M.; Llobet, A.; Parella, T.; Benet-Buchholz, J. *J. Am. Chem. Soc*., **2004,** 126, 7798-7799.

[49] Romero, I.; Rodriguez, M.; Sens, C.; Mola, J.; Kollipara, M. R.; Francas, L.; Mas-Marza, E.; Escriche, L; Llobet, A. *Inorg. Chem*., **2008**, 47, 1824-1834.

[50] Geletii, Y. V.; Huang, Z.; Hou, Y.; Musaev, D. G.; Lian, T.; Hill, C. L. *J. Am. Chem. Soc*., **2009,** 131, 7522-7523.

[51] Chronister, C. W.; Binstead, R. A.; Ni, J.; Meyer, T. J. *Inorg. Chem*., **1997**, 36, 3814-3815.

[52] Lebeau, E. L.; Adeyemi, A. A.; Meyer, T. J. *Inorg. Chem*., **1998**, 37, 6476-6484.

[53] Concepcion, J. J.; Jurss, J. W.; Templeton, J. L.; Thomas, J. M. *J. Am. Chem. Soc*., **2008,** 130, 16462-16463.

[54] Bozoglian, F.; Romain, S.; Ertem, M. Z.; Todorova, T. K.; Sens, C.; Mola, J.;

Rodriguez, M.; Romero, I.; Benet-Buchholz, J.; Fontrodona, X.; Cramer, C. J.; Gagliardi, L.; Llobet, A. *J. Am. Chem. Soc*., **2009,** 131, 15176-15187.

[55] Sjodin, M.; Styring, S.; Åkermark B.; Sun, L-C.; Hammarström, L. *J. Am. Chem. Soc*., **2000,** 122, 3932-3936.

[56] Soper, J. D.; Kryatov, S. V.; Rybak-Akimova, E. V.; Nocera, D. G. *J. Am. Chem. Soc*., **2007**, 129, 5069-5075.

[57] Hammes-Schiffer, S. *Acc. Chem. Res.* **2009**, 42, 1881-1889.

[58] Sjodin, M.; Styring, S.; Åkermark, B.; Sun, L, Hammarström, L. *J. Am. Chem. Soc*., **2000**, 122, 3932-3936.

[59] Magnuson, A.; Berglund, H.; Korall, P.; Hammarström, L.; Åkermark, B.; Styring, S.; Sun, L. *J. Am. Chem. Soc*., **1997**, 119, 10720-10725.

[60] Yeager, E. *J Mol Catal.*, **1986**, 38, 5-25.

[61] Bard, A. J.; Faulkner, L. R.; *Electrochemical methods: fundamentals and applications*. New York, Wiley, **1980**.

[62] Meyer, T. J.; Huynh, M. H. V. *Inorg. Chem*., **2003**, 42, 8140-8160.

[63] Eggleston, D. S. Goldsby, K. A.; Hodgson, D. J.; Meyer, T. J. *Inorg. Chem*., **1985**, 24, 4573-4580.

[64] Moyer, B. A.; Meyer, T. J. *J. Am. Chem. Soc*., **1978**, 100, 3601-3603.

[65] Concepcion, J. J.; Jurss, J. W.; Templeton, J. L.; Meyer, T. J. *Proc. Natl. Acad. Sci*. U.S.A., **2008**, 105, 17632-17635.

[66] Gersten, S. W.; Samuels, G. J.; Meyer, T. J. *J. Am. Chem. Soc*., **1982,** 104, 4029-4030.

[67] Gilbert, J. A.; Eggleston, D. S.; Murphy, W. R.; Geselowitz, D. A.; Gersten, S. W.; Hodgson, D. J.; Meyer, T. J. *J. Am. Chem. Soc*., **1985,** 107, 3855-3864.

[68] Kaveevivitchai, N.; Zong, R.; Tseng, H-W.; Chitta, R.; Thummel. R. P. *Inorg. Chem*., **2012**, 51, 2930-2939.

[69] Deng, Z.; Tseng, H-W.; Zong, R.; Wang, D.; Thummel, R. *Inorg. Chem*., **2008**, 47, 1835-1848.

[70] Tseng, H-W.; Zong, R.; Muckerman, J. T.; Thummel, R. *Inorg. Chem*., **2008**, 47, 11763-11773.

[71] Zong, R.; Thummel. R. P. *J. Am. Chem. Soc*., **2005,** 127, 12802-12803.

[72] Xu, Y.; Åkermark, T.; Gyollai, V.; Zou, D.; Eriksson, L.; Duan, L.; Zhang, R.; Åkermark, B.; Sun, L. *Inorg. Chem*., **2008**, 48, 2717-2719.

[73] Duan, L.; Xu, Y.; Zhang, P.; Wang, M.; Sun, L-C. *Inorg. Chem*., **2010**, 49, 209-215.

[74] Duan, L.; Fischer, A.; Xu, Y.; Sun, L-C. *J. Am. Chem. Soc*., **2009,** 131, 10397-10399.

[75] Duan, L.; Xu, Y.; Tong, L.; Sun, L-C. *ChemSusChem.*, **2011**, 4, 238-244.

[76] a) Blakemore, J. D.; Schley, N. D.; Balcells, D.; Hull, J. F.; Olack, G. W.; Incarvito, C. D.; Eisenstein, O.; Brudvig, G. W.; Crabtree, R. H. *J. Am. Chem. Soc*., **2010,** 132, 16017-16029. b) McDaniel, N. D.; Coughlin, F. J.; Tinker, L. L.; Bernhard, D. *J. Am. Chem. Soc*., **2008,** 130, 210-217.

[77] Codolà, Z.; Cardoso, J. M. S.; Royo, B.; Costas, M.; Fillol, J. L. *Chem. Eur. J*. **2013**, 19, 7203-7213.

[78] Tagore, R.; Crabtree, R. H.; Brudvig, G. W. *Inorg. Chem*., **2008**, 47, 1815-1823.

[79] a) Dogutan, D. K.; McGuire, Jr, R.; Nocera, D. G. *J. Am. Chem. Soc*., **2011,** 133, 9178-9180; b) Poater, A., *Catal. Commun*., **2014**, 44, 2-5. c) Enthaler, S.; Junge, K.; Beller, M., *Angew. Chem. Int. Ed*. **2008**, 47, 3317-3321; d)Fillol, J. L.; Codolà, Z.; Garcia-Bosch, I.; Gomez, L.; Pla, J. J.; Costas, M., *Nat. Chem.*, **2011**, 3, 807-813.

[80] a) Barnett, S. M.; Goldberg, K. I.; Mayer, J. M. *Nat. Chem*. **2012**, 4, 498-502; b) Lewis, E. A.; Tolman, W. B. *Chem. Rev*. **2004**, 104, 1047–1076; c) Mirica, L. M., Ottenwaelder, X.; Stack, T. D. P. *Chem. Rev*. **2004**, 104, 1013–1046; d) Maiti, D., Woertink, J. S., Narducci Sarjeant, A. A., Solomon, E. I., Karlin, K. D. *Inorg. Chem*. **2008**, 47, 3787–3800.

[81] a) Umena, Y.; Kawakami, K.; Shen, J. R.; Kamiya, N. *Nature*, **2011**, 473, 55-60. b) Polander, B. C.; Barry, B. A. *Proc. Natl. Acad. Sci*. U.S.A., **2012**, 109, 1-6.

[82] Tong, L.; Wang, Y.; Duan, L.; Xu, Y.; Cheng, X.; Fischer, A.; Ahlquist, M. S. G.; Sun, L. *Inorg. Chem.*, **2012**, *51*, 3388–3398.

[83] Romain, S.; Vigara, L.; Llobet, A. *Acc. Chem. Res*., **2009**, 42, 1944-1953.

[84] Muckerman, J. T.; Polyansky, D. E.; Wada, T.; Tanaka, K.; Fujita, E. *Inorg. Chem*., **2008**, 47, 1787-1802.

[85] Betley, T. A.; Wu, Q.; Voorhis, T. V.; Nocera, D. G. *Inorg. Chem*., **2008**, 47, 1849-1861.

[86] Liu, X.; Wang, F. Y. *Coord. Chem. Res*., **2012**, 256, 1115-1136.

[87] Vrettos, J. S.; Limburg, J.; Brudvig, G. W. *Biochimica ET Biophysica ACTA-Bioenergetics*, **2001**, 1503, 229-245.

[88] Concepcion, J. J.; Jurss, J. W.; Brennaman, M. K.; Hoertz. P. G.; Patrocinio, A. O. T.; Iha, N. Y. M.; Templeton, J. L.; Thomas, J. M. *Acc. Chem. Res*., **2009**, 42, 1954-1965.

[89] Liu, F.; Concepcion, J. J.; Jurss, J. W.; Cardolaccia, T.; Templeton, J. L.; Thomas, J. M. *Inorg. Chem*., **2008**, 47, 1727-1752.

[90] Ref. Concepcion, J. J.; Jurss, J. W.; Templeton, J. L.; Meyer, T. J. *Proc. Natl. Acad. Sci*. U.S.A, **2008**, 105, 17632-17635.

[91] Bozoglian, F.; Romain, S.; Ertern, M. Z.; Todorava, T. K.; Sens, C.; Mola, J.; Rodriguez, M.; Romero, I.; Benet-Buchholz, J.; Fontrodona, X.; Cramer, C. J.; Gagliardi, L.; Llobet, A. *J. Am. Chem. Soc*., **2009,** 131, 15176-15187.

[92] Nyhlen, J.; Duan, L.; Åkermark, B.; Sun, L-C.; Privalov, T. *Angew. Chem. Int. Ed*., **2010**, 49, 1773-1777.

[93] Duan, L.; Bozoglian, F.; Mandal, S.; Stewart, B.; Privalov, T.; Llobet, A.; Sun, L-C. *Nat. Chem.*, **2012**, 4, 418-423.

[94] Dismukes, G. C. *Acc. Chem. Res.,* **2009**, 42, 1935-1943.

[95] Lundberg, M.; Blomberg, M. R. A.; Siegbahn, P. E. M. *Inorg. Chem*., **2004**, 43, 264-274.

[96] Siegbahn, P. E. M.; Crabtree, R. H. *J. Am. Chem. Soc*., **1999,** 121, 117-127.

[97] Yang, X.; Baik, M. H. *J. Am. Chem. Soc*., **2006,** 128, 7476-7485.

[98] Liumburg, J.; Vrettos, J. S.; Liable-Sands, L. M.; Rheingold, A. L.; Crabtree, R, H.; Brudvig, G. W. *Science*, **1999**, 283, 1524-1527.

[99] Yang, X, Baik, M. H. *J. Am. Chem. Soc*., **2008,** 130, 16231-16240.

[100] Turner, J. A. *Science.*, **2004**, 305, 972-974.

[101] Lubitz, W.; Tumas, B. *Chem. Rev.*, **2007**, 107, 3900-3903.

[102] Zittel, Werner & Wurster, Reinhold & Bolkow, Ludwig. *Advantages and Disadvantages of Hydrogen. Hydrogen in the Energy Sector. Systemtechnik*

Gmbitt., **1996**.

[103] Mikkelsen, R. L.; Bruulsema, T. W. *HortTechnology.*, **2005**, 15, 24-30.

[104] Watt, J. G. *CIM. Bull.,* **2003**, 96, 84-88.

[105] Delmon, B. *Catal Lett*., **1993**, 22, 1-32.

[106] Siegbahn, P. E. M.; Tye, J. W.; Hall, M. B. *Chem. Rev.*, **2007**, 107, 4414-4435.

[107] Hess, R.; Vargas, A.; Mallat, T.; Burgi, T.; Baiker, A. *J. Catal.*, **2004**, 222, 117-128.

[108] Arx, M.; Mallat, T.; Baiker, A. *Angew. Chem. Int. Ed*., **2001**, 40, 2302-2305.

[109] Frey, M. *ChemBioChem.*, **2002**, 3, 153-160.

[110] Wu, L-F.; Mandrand, M. A. *FEMS Microbiol. Rev.*, **1993**, 104, 243-270.

[111] Hahn, D.; Kuck, U. *Process. Biochem.*, **1994**, 29, 633-644.

[112] Okura, I. *Coord. Chem. Res.*, **1985**, 68, 53-99.

[113] Shima, S.; Thauer, R. K. *Chem. Rec.*, **2007**, 7, 37-46.

[114] Brown, J. R.; Doolittle, W. F. *Microbiol. Mol. Biol. Rev.*, **1997**, 61, 456-502.

[115] Leonard, C. J.; Aravind, L.; Koonin, E. V. *Genome Res.*, **1998**, 8, 1038-1047.

[116] Ogata, H.; Mizoguchi, Y.; Mizuno, N.; Miki, K.; Adachi, S.; Yasuoka, N.; Yagi, T.; Yamauchi, O.; Hirota, S.; Higuchi, Y. *J. Am. Chem. Soc*., **2002**, 124, 11628-11635.

[117] Casalot, L.; Rousset, M. *Trends. Microbiol.*, **2011**, 9, 228-237.

[118] Volbeda, A.; Charon, M. H.; Piras, C.; Hatchikian, E. C.; Frey, M.; Fontecilla-Camps, J. C. *Nature*, **1995**, 373, 580-587.

[119] Volbeda, A.; Martin, L.; Cavazza, C.; Matho, M.; Faber, B. W.; Roseboom, W.; Albracht, S. P. J.; Garcin, E.; Rousset, M.; Fontecilla-Camps, J. C. *J. Biol. Inorg. Chem.*, **2005**, 10, 239-249.

[120] Volbeda, A.; Garcin, E.; Pira, C.; Lacey, A. L.; Fernadez, V. M.; Hatchikian, E. C.; Frey, M.; Fontecilla-Camps, J. C. *J. Am. Chem. Soc*., **1996**, 118, 12989-12996.

[121] Higuchi, Y.; Yagi, T.; Yasuoka, N. *Structure.*, **1997**, 5, 1671-1680.

[122] Lacey A. L. D.; Fernández, V. M.; Rousset, M.; Cammack, R. *Chem. Rev.*, **2007**, 107, 4304-4330.

[123] Nicolet Y.; Cavazza, C.; Fontecilla-Camps, J. C. *J. Inorg. Biochem.*, **2002**, 91, 1-8.

[124] Peters, J. W. *Curr. Opin. Struct. Biol.,* **1999**, 9, 670-676.

[125] Corr, M. J.; Murphy, J. A. *Chem. Soc. Rev*. **2011**, 40, 2279-2292.

[126] Meyer, J. *Cell. Mol. Life Sci.*, **2007**, 64, 1063-1084.

[127] Peters, J. W.; Lanzilotta, W. N.; Lemon, B. J.; Seefildt, L. C. *Science*, **1998**, 282,1853-1858.

[128] Pandey, A. S.; Harris, T. V.; Giles, L. J.; Peters, J. W.; Szilagyi, R. K. *J. Am. Chem. Soc*., **2008**, 130, 11106-11113.

[129] Armstrong, F. A. *Curr Opin Struct Biol.*, **2004**, 8, 133-140.

[130] Tye, J. W.; Hall, M. B.; Darensbourg, M. Y. *Proc. Natl. Acad. Sci*. U.S.A. **2005**, 102, 16911-16912.

[131] Fan, H. J.; Hall, M. B. *J. Am. Chem. Soc*., **2001**, 123, 3828-3829.

[132] Felton, G. A. N.; Vannucci, A. K.; Chen, J.; Lockett, L. T.; Okumura, N.; Petro, B. J.; Zakai. U. I.; Evans D. H.; Glass, R. S.; Lichtenberger, D. L. *J. Am. Chem. Soc*., **2007**, 129, 12521-12530.

[133] Zhao, X.; Georgakaki, I. P.; Miller, M. L.; Mejia-Rodriguez, R.; Chiang, C. Y.; Darensbourg, M. Y. *Inorg. Chem*., **2002**, 41, 3917-3928.

[134] Curtis, C. J.; Miedaner, A.; Ciancanelli, R.; Ellis, W. W.; Noll, B. C.; DuBois, M. R.; DuBois, D. L. *Inorg. Chem*., **2003**, 42, 216-227.

[135] Barton, B. E.; Rauchfuss, T. B. *Inorg. Chem*., **2008**, 47, 2261-2263.

[136] Gloaguen, F.; Lawrence, J. D.; Rauchfuss, T. B. *J. Am. Chem. Soc*., **2001**, 123, 9476-9477.

[137] Li, P.; Wang, M.; He, C.; Li, G.; Liu, X.; Chen, C.; Åkermark, B.; Sun, L-C. *Eur. J. Inorg. Chem.*, **2005**, 2506-2513.

[138] Wang, N.; Wang, M.; Zhang, T.; Li, P.; Liu, J.; Sun, L-C. *Chem. Commun*., **2008**, 5800-5802.

[139] Augugliaro, V.; Loddo, V.; Palmisano, L.; Schiavello, M. *J. Catal*., **1995**, 153, 32-40.

[140] Siemon, U.; Bahnemann, D.; Testa, J. J.; Rodriguez, D.; Litter, M. I.; Bruno, N. *J. Photochem. Photobiol., A: Chemistry*, **2002**, 148, 247-255.

[141] Serprone, N.; Salinaro, A. *Pure & Appl. Chem.*, **1999**, 71, 303-320.

[142] Na, Y.; Pan, J.; Wang, M.; Sun L-C. *Inorg. Chem*., **2007**, 46, 3813-3815.

[143] Na, Y.; Wang, M.; Pan, J.; Zhang, P.; Åkermark, B.; Sun L-C. *Inorg. Chem*., **2008**, 47, 2805-2810.

[144] Wang, M.;Chen, L.; Li, X.; Sun L-C. *J. Chem. Soc, Dalton Trans.*, **2011**, 40, 12793-12800.

[145] Du, P.; Knowles, L.; Eisenberg, R. *J. Am. Chem. Soc*., **2008**, 130, 12576-12577.

[146] Wang, F.; Wang, W.; Wang, X.; Yang, H.; Tung, C.; Wu, L. *Angew. Chem. Int. Ed*., **2011**, 50, 3193-3197.

[147] Wang, M.; Na, Y.; Gorlov, M.; Sun L-C. *Dalton Trans.*, **2009**, 6458-6467.

[148] Kaila, V. R. I.; Verkhovsky, M. I.; Wikström, M. *Chem. Rev.*, **2010**, 110, 7062-7081.

[149] Xu, J.; Voth, G. A. *Proc. Natl. Acad. Sci*. U.S.A., **2005**, 102, 6795-6800.

[150] Ketchem, R. R.; Hu, W.; Cross, T. A. *Science*, **1993**, 261, 1457-1460.

[151] Roux, B. *Acc. Chem. Res*., **2002**, 35, 366-375.

[152] Wang, Y.; Wang, M.; Sun, L.; Ahlquist, M. S. G. *Chem. Commun*., **2012**, 4450-4452.

[153] Henry, R. M.; Shoemaker, R. K.; Dubois, D. L. DuBois, M. R. *J. Am. Chem. Soc*., **2006**, 128, 3002-3010.

[154] O'Hagan, M.; Shaw, W. J.; Raugei, S.; Chen, S.; Yang, J. Y.; Kilgore, U. J.; DuBois, D. L.; Bullock, R. M. *J. Am. Chem. Soc*., **2011**, 133, 14301-14312.

[155] Yang, J. Y.; Bullock, R. M.; Shaw, W. J.; Twamley, B.; Fraze, K.; DuBois, M. R.; DuBois, D. L.; *J. Am. Chem. Soc*., **2009**, 131, 5935-5945.

[156] Ezzaher, S.; Capon, J. F.; Gloaguen, F.; Petillon, F. Y.; Schollhammer, P.; Talarmin, J. *Inorg. Chem*., **2009**, 48, 2-4.

[157] Wang, N.; Wang, M.; Liu, J.; Jin, K.; Chen, L.; Sun, L-C. *Inorg. Chem*., **2009**, 48, 11551-11558.

[158] Wang, Z.; Liu, J-H.; He, C-J.; Jiang, S.; Åkermark, B.; Sun, L-C. *J.*

Organomet Chem., **2007**, 692, 5501-5507.

[159] Barton, B. E.; Olsen, M. T.; Rauchfuss, T. B. *J. Am. Chem. Soc*., **2008**, 130, 16834-16835.

[160] Camara, J. M.; Rauchfuss, T. B. *J. Am. Chem. Soc*., **2011**, 133, 8098-8101.

[161] Wang, N.; Wang, M.; Wang, Y.; Zheng, D.; Han, H.; Ahlquist, M.; Sun, L-C. *J. Am. Chem. Soc.*, **2013**, 135, 13688-13691.

[162] Carroll, M. E.; Barton, B. E.; Rauchfuss, T. B.; Carroll, P. J. *J. Am. Chem. Soc.*, **2012**, 134, 18843-18852.